*materials*

MDPI

*Article*

# Conservation Environments' Effect on the Compressive Strength Behaviour of Wood–Concrete Composites

**Walid Khelifi [1], Selma Bencedira [2,*], Marc Azab [3], Malik Sarmad Riaz [4], Mirvat Abdallah [3], Zaher Abdel Baki [3], Andrey E. Krauklis [5] and Hani Amir Aouissi [6]**

[1] Laboratory of Civil Engineering, Department of Civil Engineering, Faculty of Technology, UBMA, Annaba 23000, Algeria; khelifi.walid23@gmail.com
[2] Laboratory of LGE, Department of Process Engineering, Faculty of Technology, UBMA, B. P12, Annaba 23000, Algeria
[3] College of Engineering and Technology, American University of the Middle East, Kuwait; marc.azab@aum.edu.kw (M.A.); mirvat.abdallah@aum.edu.kw (M.A.); zaher.abdelbaki@aum.edu.kw (Z.A.B.)
[4] Civil Engineering Department—National University of Technology (NUTECH), Islamabad, Pakistan; sarmadriaz@nutech.edu.pk
[5] Institute for Mechanics of Materials, University of Latvia, Jelgavas Street 3, LV-1004 Riga, Latvia; andrejs.krauklis@lu.lv
[6] Scientific and Technical Research Center on Arid Regions (CRSTRA), Biskra 07000, Algeria; aouissi.amir@gmail.com
* Correspondence: selmaben30@yahoo.fr

**Abstract:** This paper addresses the issues in making wood–concrete composites more resilient to environmental conditions and to improve their compressive strength. Tests were carried out on cubic specimens of 10 × 10 × 10 $cm^3$ composed of ordinary concrete with a 2% redwood- and hardwood-chip dosage. Superficial treatments of cement and lime were applied to the wood chips. All specimens were kept for 28 days in the open air and for 12 months in: the open air, drinking water, seawater, and an oven. Consequently, the compressive strength of ordinary concrete is approximately 37.1 MPa. After 365 days of exposure to the open air, drinking water, seawater, and the oven, a resistance loss of 35.84, 36.06, 42.85, and 52.30% were observed, respectively. In all environments investigated, the untreated wood composite concrete's resistance decreased significantly, while the cement/lime treatment of the wood enhanced them. However, only 15.5 MPa and 14.6 MPa were attained after the first 28 days in the cases of the redwood and the hardwood treated with lime. These findings indicate that the resistance of wood–concrete composites depends on the type of wood used. Treating wood chips with cement is a potential method for making these materials resistant in conservation situations determined by the cement's chemical composition. The current study has implications for researchers and practitioners for further understanding the impact of these eco-friendly concretes in the construction industry.

**Keywords:** renewable materials; wood cuttings; vegetal fibre concrete; compressive strength; mechanical behaviours; experimentation

check for updates

**Citation:** Khelifi, W.; Bencedira, S.; Azab, M.; Riaz, M.S.; Abdallah, M.; Abdel Baki, Z.; Krauklis, A.E.; Aouissi, H.A. Conservation Environments' Effect on the Compressive Strength Behaviour of Wood–Concrete Composites. *Materials* **2022**, *15*, 3572. https://doi.org/10.3390/ma15103572

Academic Editors: Wei Zhou and Qiao Wang

Received: 7 April 2022
Accepted: 12 May 2022
Published: 17 May 2022

**Publisher's Note:** MDPI stays neutral with regard to jurisdictional claims in published maps and institutional affiliations.

**Copyright:** © 2022 by the authors. Licensee MDPI, Basel, Switzerland. This article is an open access article distributed under the terms and conditions of the Creative Commons Attribution (CC BY) license (https://creativecommons.org/licenses/by/4.0/).

## 1. Introduction

The construction sector directly contributes to the expansion of economic activities while, at the same time, it is a major consumer of natural and physical resources. Unfortunately, this expansion has adverse environmental, social, and economic impacts. The environmental impact of construction activities has increased in recent decades due to the rapid increases in the population and greater industrial activity [1,2]. The building industry is responsible for around a quarter of all $CO_2$ emissions [3], not to mention the loss of non-renewable resources [4]. As a result, the building industry must innovate to ensure customer satisfaction, while also being environmentally sustainable, hence the interest in creating an eco-construction technique [5–7]. This unique design technique strives to

produce pleasant structures at a reduced environmental cost by using more efficient materials [8]. In this context, agro-materials, partially produced from biomass [9], are rapidly being developed and commercialized in the construction materials market [10,11]. Because of their ecological nature, these agro-materials make it possible to enhance the environmental balance of construction, particularly of buildings [12–15]. Among the agro-materials, vegetable concretes have been designed to be used in the construction industry [16,17] to take advantage of their thermal, acoustic, and hygroscopic qualities [18,19]. These concretes generally encourage the recovery of by-products from different economic sectors. Academics and practitioners have shown interest in investigating and comprehending these materials in the presence of various stressors [20]. Plant or cellulose fibres (CFs) are the most-often utilized vegetable concretes [21,22] as they are characterized by low cost, light weight, good adhesion, a simple production method, and biodegradability, which is attracting the attention of an increasing number of researchers.

Cellulose fibre (CF) is one of the world's most plentiful natural resources, and it may be found in a variety of agricultural leftovers, including rice straw, rice husk, maize straw, bagasse, wood shavings, wood chips, bamboo chips, and so on [23,24]. These agricultural wastes are mostly made up of cellulose, hemicellulose, lignin, pectin, wax, and other water-soluble components [25]. CF is essentially identical, with slight density variations between 1.1 and 1.6 g $cm^{-3}$. For example, softwood has a density of roughly 1.5 g $cm^{-3}$, a reasonably high tensile strength, and a comparatively low tensile strength compared to fruit coconut-husk fibre [26]. Most of this field's research has focused on cementitious wood-composite panels based on pervious concrete. Cement-bonded–wood-fibre composites are not new in the building industry [27,28]. These materials are less harmful to the environment and less expensive to manufacture. They have a thermal conductivity similar to expanded polystyrene and glass wool [29,30]. In addition, fibre-based composite materials have sparked fresh attention because of their potential to adjust interior climates [31]. Numerous investigations have demonstrated that the hygroscopic behaviour of materials of vegetable origin allows for the regulation of ambient humidity [32]. In addition, they can be easily employed for both new construction and renovations [33]. They also offer additional benefits, such as good phonic insulation due to their ability to absorb sound waves [34–36]. Another significant advantage of using wood filler in cementitious materials is its cost; it is readily accessible, ecologically acceptable, and simple to process [37–39]. However, the primary challenges faced throughout numerous studies of wood–concrete products have been the compressibility of the wood particles inside the hardened concrete due to their low level of stiffness [40] and the incompatibility induced by soluble chemicals during the fresh cement phase [41]. In fact, they can raise the pH of the cement mixture over 12.5 due to the creation of $Ca(OH)_2$, which aids in dissolving low-molecular-weight compounds inside the wood particles. As a result, the wood particles must be treated before being employed in the concrete composite [42]. Table 1 summarizes the many ways generally used for the treatment of wood. The coating technique is a typical treatment method for minimizing the influence of soluble chemicals while also boosting volume stability and surface roughness [43].

Thus, an experimental approach, developed by Khelifi et al. [49], was performed to assess the thermo-mechanical properties of treated/untreated wood-chip-concrete. The utilised redwood and hardwood chips were obtained from carpentry waste, namely trash from routing and planning work. The utilised redwood and hardwood chips were treated with cement and lime. The experimental research findings for the concrete properties demonstrate the higher performance of the examined concrete compared to composite concrete made with untreated wood chips. The treatment enhances the adhesion of the wood matrix. Ordinary concrete can benefit from the addition of wood chips to improve its heat conductivity. This improvement of construction material made from renewable resources has the potential to provide high thermal insulation. However, until specific issues impeding their utilisation are addressed, the use of wood–concrete materials in the building industry will remain limited. In addition, all of the data were obtained just after

the material's cement hardened (after 28 days in the open air). If they are to be employed as structural elements, their mechanical properties must be improved. They must also withstand the conditions imposed by the environments in which they will be utilized for as long as possible. Due to the complexities of the effects involved in this investigation, only compressive strength will be evaluated. Finally, this research will fill the gap in the literature regarding the effect of adding wood chips to concrete paste by addressing the following questions:

1. How does ordinary concrete compressive strength behave in storage environments?
2. What effects do treated/untreated wood chips have on this behaviour?
3. Does the type of wood influence this behaviour?
4. How does the chemical composition of the cement used in wood-chip treatments contribute to the composite's resistance to various storage conditions?

**Table 1.** Treatment methods for wood.

| Treatment Methods | Advantage | Techniques | References |
|---|---|---|---|
| Thermal | Thermal modifications are the chemical and physical changes that occur in natural fibres because of temperature applications, where different process factors substantially impact fibre qualities. | Hornification<br>Heat<br>Hydrothermal | [44,45] |
| Chemical | These treatments eliminate contaminants from the surface of natural fibres, enhancing fibre–matrix adhesion. | Alkali<br>Saline<br>Formaldehyde | [25,46] |
| Coating | This reduces the impact of soluble compounds while increasing volume stability and surface roughness. | Linseed oil<br>Cement<br>Lime | [47] |
| Biological | Environmentally friendly fibre modification approaches, low-energy processing, softer reaction conditions, the ability to deploy recycling systems, and enhanced fibre characteristics were accomplished. | Enzymes<br>Fungi<br>Bacteria | [47,48] |

## 2. Materials and Methods

### *2.1. Research Methodology*

Figure 1 depicts the itemized, strategic system for the development of the compressive strength investigation of cement materials made from redwood and hardwoods. After being preserved in multiple environments, specimens underwent compressive strength studies. Those specimens were made of ordinary concrete and treated/untreated wood–concrete composites. There were two types of wood used: redwood and hardwood. The treatment of wood chips can take several forms; in this investigation, the wood chips were coated with cement and lime. The duration and the conservation environments were as follows: 28 days in the open air and then 365 days in: (i) open air, (ii) seawater, (iii) drinking water, and (iv) an oven.

The steps mentioned above were followed to develop the ordinary concrete and the treated/untreated-wood concrete using established concept development and strength analysis.

### *2.2. Materials*

The shavings were by-products of woodworking processes. Redwood ($W_I$) was produced from the wood of a Scots pine tree. According to NF EN 1611 European classification standards, $W_I$ is classified as VI Scandinavian. Hardwood ($W_{II}$) was steamed beech sawn from Romania. European standard NF EN 975-1 classifies $W_{II}$ as a pedunculated oak species. Both of them have rapid growth and are cost-effective; these species of wood are widely employed in the construction sector. Both are distinguished by rapid development and low-cost aggregates. $W_{II}$ has higher mechanical properties than $W_I$.

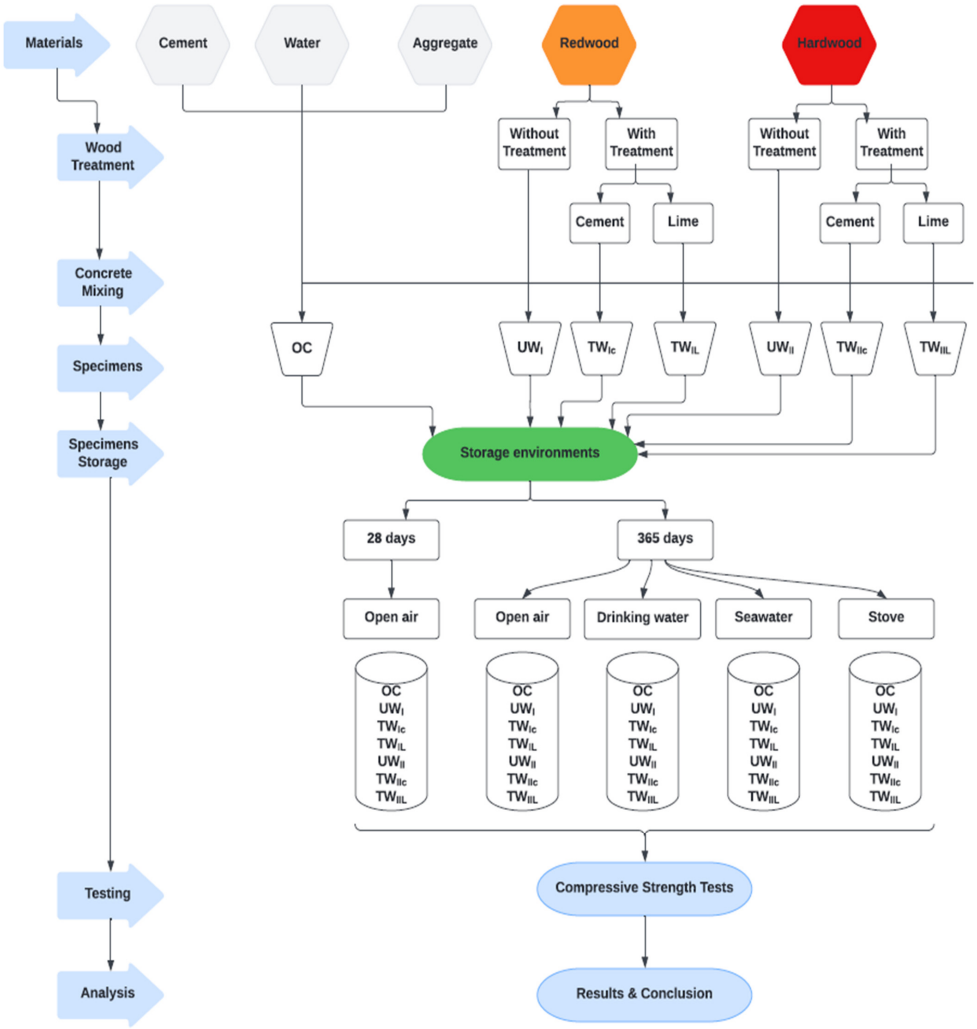


**Figure 1.** Methodological framework.

The density at RH 15% is typically 0.1 for redwood and 0.3 to 0.4 for hardwood. Both, measuring 0.5–12.5 mm, had an irregular form [49]. It should be ensured that the chips are evenly dispersed in the cement matrix throughout the mixing process.

The multiple grain sizes that make up a sample may be determined and seen via granulometric analysis. The granulometric analysis is performed using a LATEST SPA sieve machine set to moderate vibration. The study entailed sorting and categorising the grains based on their diameter using sieves piled one on top of the other, with the diameters of the holes decreasing from top to bottom. In general, the sample analysed in this study was placed on the top sieve, and the categorisation of the grains was acquired by the vibration of the sieve column. The column was stirred mechanically. The sieves were then agitated one by one, starting with the one with the widest opening, and using a bottom and a cover. When the residue did not change by more than 1% after one minute of sifting, the sieving was complete. The refuse was passed through each sieve, and the results were added together. Figure 2 shows the chip granulometric curves of $W_I$ and $W_{II}$. It clearly shows that the wood chips had an irregular form, a higher granulometric limit of approximately 12.5 mm, and a lower granulometric limit of approximately 0.5 mm. Because of the chips' lack of stiffness and geometry, none of these characteristics was of any relative value.

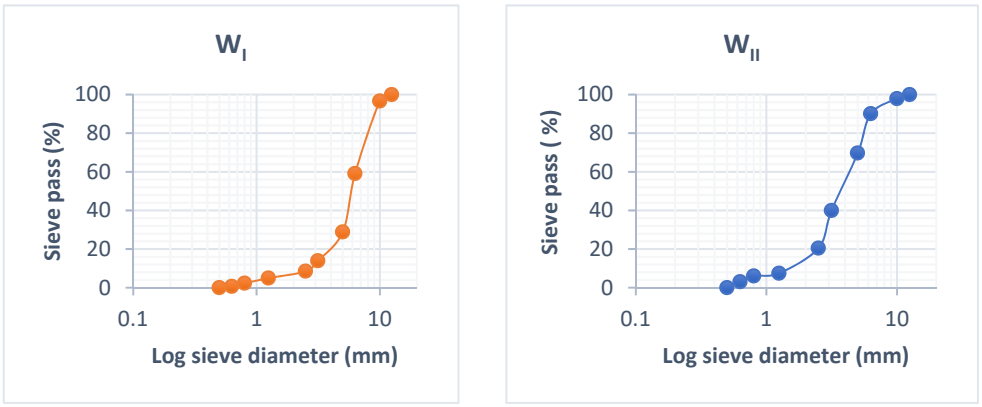


**Figure 2.** Wood ($W_I$ and $W_{II}$) chip granulometric curves.

The method appeared to be adequate for supplementing scanning electron microscopy (SEM) of surface features. Therefore, SEM analyses of wood-chip samples were performed using a JEOLJSM100F spectrophotometer. Figures 3 and 4 show SEM microstructural images of $W_I$ and $W_{II}$ for various view fields ranging from 10 µm to 500 µm. From Figure 3, we can see that $W_I$ chips have a fibrous texture with ordered distribution, while Figure 4 shows the ordered distribution of $W_{II}$'s fibrous texture. Despite this fact, the $W_I$ and $W_{II}$ are rather compact materials with fibres that run in the same direction.

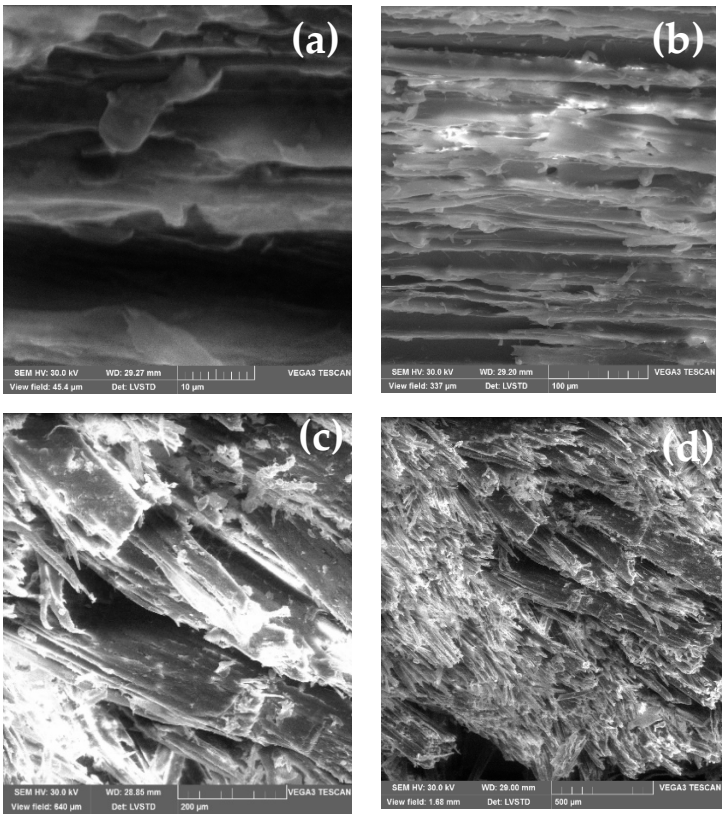


**Figure 3.** SEM microstructural images of $W_I$ for various view fields: (**a**) 10 µm, (**b**) 100 µm, (**c**) 200 µm, and (**d**) 500 µm.

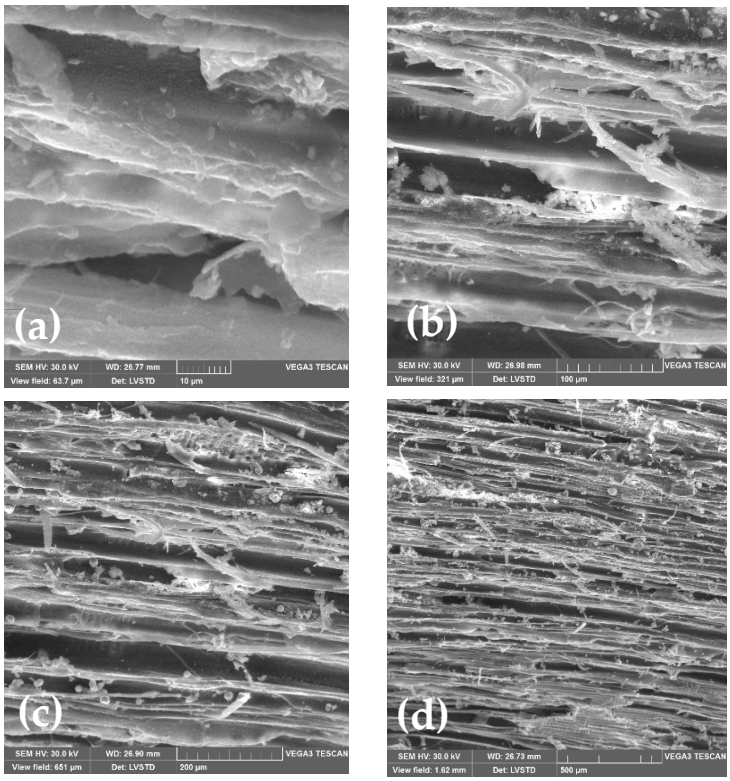


**Figure 4.** SEM microstructural images of $W_{II}$ for various view fields: (**a**) 10 µm, (**b**) 100 µm, (**c**) 200 µm, and (**d**) 500 µm.

The geometrical dimensions of the wood chips may also be seen in the SEM pictures. According to SEM examination, the wood chips had a low recovery property.

Portland cement (type II) class 45 (CPJ-CEM II/A) was utilized with the following physical characteristics: a specific surface area of 289 $m^2$ $kg^{-1}$, a specific density of 3078 kg $m^{-3}$, and a loss on ignition of 1.16%. Tables 2 and 3 show the mineralogical and chemical compositions of the cement, respectively. The Bogue method was used to determine both of these at the Hadjar Essoud (Skikda, Algeria) cement plant laboratory. Table 2 shows the chemical compositions as determined by the Hadjar Essoud [50] (Skikda, Algeria) cement plant laboratory (SCHS), from which the used Portland cement was obtained. On the other hand, Table 3 shows the mineralogical composition of the cement. It is derived from the data in Table 2 using the Bogue calculation [51]. In fact, the Bogue method was used to approximate the proportions of the four primary minerals in the Portland cement clinker [52]. Despite the fact that the results are only approximate, the computation is incredibly valuable and commonly used in the cement industry. The calculation assumes that the primary clinker minerals are pure minerals with the following compositions: (i) alite or tricalcium silicate ($C_3S$); (ii) belite or dicalcium silicate ($C_2S$); (iii) tricalcium aluminate ($C_3A$); and (iv) tetracalcium aluminoferrite ($C_4AF$) [53]. These clinkers may be computed using Equations (1)–(4) [54] where the oxides reflect the weight percentages (PW) [53]:

$$C_3S = 4.0710\ CaO - 7.6024\ SiO_2 - 1.4297\ Fe_2O_3 - 6.7187\ Al_2O_3 \quad (1)$$

$$C_2S = 8.6024\ SiO_2 + 1.0785\ Fe_2O_3 + 5.0683\ Al_2O_3 - 3.0710\ CaO \quad (2)$$

$$C_3A = 2.6504\ Al_2O_3 + 1.6920\ Fe_2O_3 \quad (3)$$

$$C_4AF = 3.0432\ Fe_2O_3 \quad (4)$$

**Table 2.** Chemical composition of the Portland cement.

| Elements | CaO | $SiO_2$ | $Al_2O_3$ | $Fe_2O_3$ | $SO_3$ | MgO |
|---|---|---|---|---|---|---|
| (%) | 60.41 | 21.91 | 5.19 | 2.94 | 1.6 | 2.19 |

*(%): Weight percentage.*

**Table 3.** Mineralogical composition of the Portland cement.

| Elements | $C_3S$ | $C_2S$ | $C_3A$ | $C_4AF$ |
|---|---|---|---|---|
| (%) | 58.2 | 18.5 | 9.3 | 8.2 |

*(%): Weight percentage.*

The concrete mixture contained 3 types of aggregates: rolling sand (2), fine aggregate (1), and coarse aggregate (3). Their mechanical and chemical characteristics are summarized in Tables 4 and 5 [49]. The aggregate characterization techniques are outlined by [55–58].

**Table 4.** Mineralogical composition of the aggregates.

| Properties | (1) | (2) | (3) | Standard |
|---|---|---|---|---|
| Apparent density (Kg $m^{-3}$) | 1380 | 1390 | 1360 | NF P 18-554 et 18-555. |
| Absolute density (Kg $m^{-3}$) | 2600 | 2450 | 2450 | NF EN 1097-3 |
| Finesses Modulus | 2.21 | - | - | NF 18-540 |
| Visual sand equivalent (%) | 84.72 | - | - | NF EN 933-8 |
| d/D | 0/5 | 3/8 | 8/16 | - |
| Fragmentation resistance (%) | - | 23 | 23 | NF P 18-573 |
| Wear resistance (%) | - | 16 | 16 | |
| Kurtosis (%) | - | 8 | 8 | NF P 18-561 |
| Water Absorption (%) | - | 0.2 | 0.2 | NF P 18-554 et 18-555 |

**Table 5.** Chemical composition of the aggregates.

| Elements | CaO | $SiO_2$ | $Al_2O_3$ | Fe | MgO | PF |
|---|---|---|---|---|---|---|
| (%) | 54.70 | 0.11 | 0.45 | 0.12 | null | 43.74 |

### *2.3. Preparation and Conditioning of Test Specimens*

#### 2.3.1. Wood Chip Treatment

Regarding the treatment of the shavings, many treatments have been utilized in earlier studies, and it has been demonstrated that treatment by coating lime with cement yields satisfactory results, particularly in terms of mechanical strength and shrinkage [59,60]. Indeed, before adding these two types of wood chips to the composition, they were immersed in the combinations (cement + water) and then (lime + water). Lime milk was made from natural hydraulic lime (NHL5). The treated chips were left to dry in their natural state for more than 3 days before use. Indeed, for cement treatment of the $W_I$ and $W_{II}$ surfaces, they are immersed individually in cement milk or in water. The cement and lime used in this operation were Portland cement and natural hydraulic lime (NHL5). Similarly, the two types of wood were immersed in cement milk for the lime treatment. Cement and lime milks are cement–water and lime–water mixtures, respectively. Both of them were prepared, respectively, with water–cement (W/C) and water–lime (W/L) ratios equal to 1. After complete saturation, the treated chips were allowed to dry in the open air for 3 days before being used. Figure 5 shows the $W_I$ and $W_{II}$ before and after the cement and lime treatments.

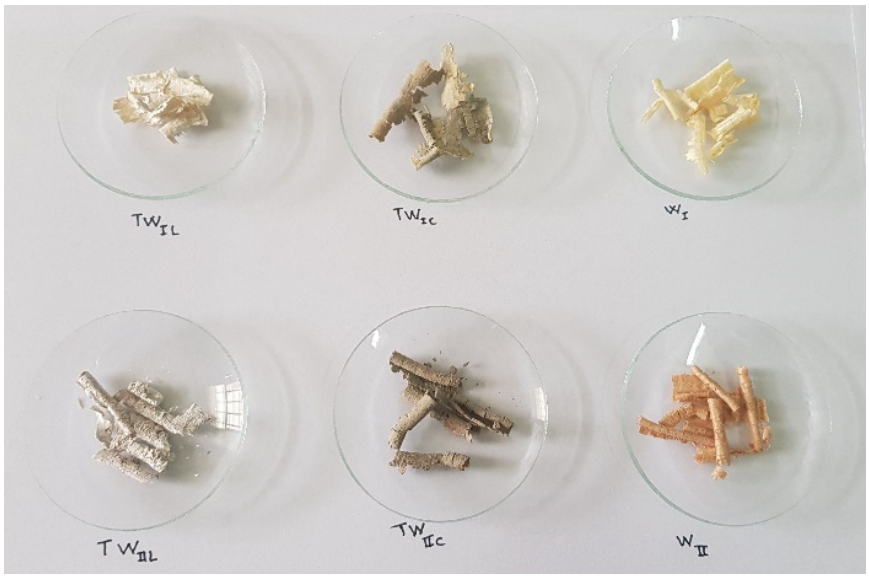


**Figure 5.** Image of $W_I$ and $W_{II}$ before and after treatment.

Seven different types of specimens will be discussed in this article:

- OC: Ordinary concrete,
- $UW_I$: Untreated redwood–cement concrete,
- $UW_{II}$: Untreated hardwood–cement concrete,
- $TW_{Ic}$: Treated redwood–cement concrete (with cement),
- $TW_{IIc}$: Treated hardwood–cement concrete (with cement),
- $TW_{IL}$: Treated redwood–cement concrete (with lime),
- $TW_{IIL}$: Treated hardwood–cement concrete (with lime).

#### 2.3.2. Formulation of Concrete

Previous research [49] has provided the ideal compositions of the sand concrete examined without including wood shavings. Indeed, concrete is a glue-based material that holds the fillers together (fine aggregates, coarse aggregates, rolling sand, and wood chips). The paste and fillers combine to form the heterogeneous substance known as "concrete." The Dreux–Gorisse technique [33] is used to investigate the concrete composition. The compositions shown in Table 6 were used to prepare the mixtures. Figure 6 shows the results of a particle size study performed on the aggregates. The aim of this formulation was to generate a common concrete with a characteristic compression resistance of 30 MPa at 28 days. The maximum diameter ($D_{max}$) was set at 1, the average vibration speed was 1, and the proportion of aggregates was as follows: 35% rolling sand, 10% fine particles, and 55% coarse aggregates (3). The compositions shown in Table 6 were used to prepare the mixtures.

**Table 6.** Formulation of concrete.

| Concrete | Cement (Kg m$^{-3}$) | Water (Kg m$^{-3}$) | E/C | (1) (Kg m$^{-3}$) | (2) (Kg m$^{-3}$) | (3) (Kg m$^{-3}$) | Chips (Kg m$^{-3}$) | Chips % |
|---|---|---|---|---|---|---|---|---|
| OC | 400 | 208 | 0.55 | 626.53 | 168.68 | 927.25 | - | 0 |
| UW | 400 | 208 | 0.55 | 614 | 165.30 | 909.2 | 34.45 | 2 |
| TW | 400 | 208 | 0.55 | 614 | 165.30 | 909.2 | 34.45 | 2 |

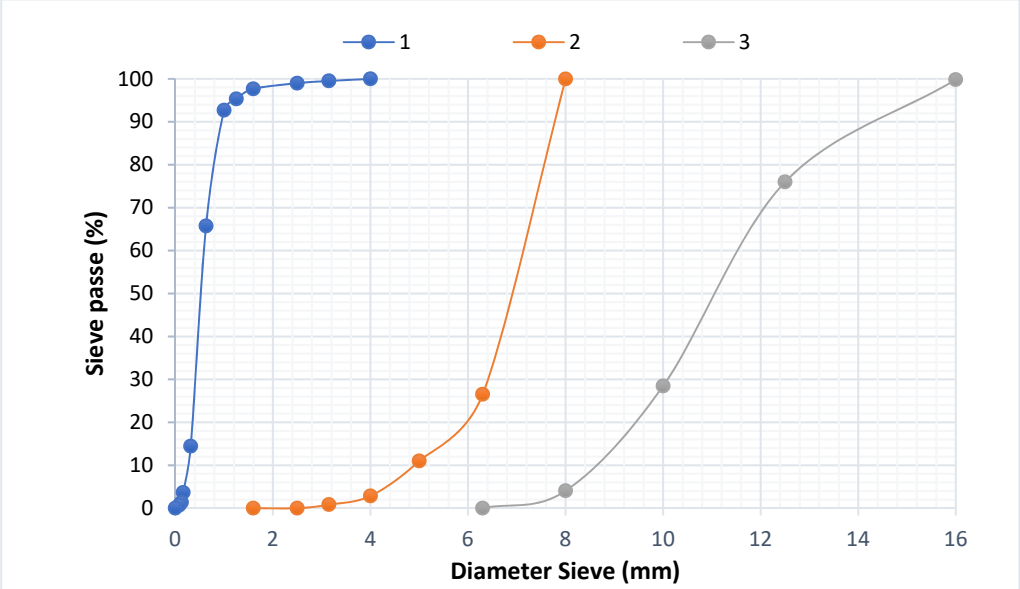


**Figure 6.** Granulometric curves and aggregate distribution graphs.

2.3.3. Concrete Mixing

These procedures are sensitive because they are required to assure the status of the coating and the holding of the chips. Therefore, a well-defined procedure and low-speed mixing (about 50 turns $mn^{-1}$) were adopted. The dry sand, cement, gravel, and wood chips were combined for 1 min at a slow speed. When the mixture was entirely homogenous, the mixing water was progressively added at a slow pace for 4 min. Using a vibrating table at a rate of 50 Hz and a vibrating time of 1 min resulted in the separation of distinct components. Finally, the moulds were manually filled.

2.3.4. Preparation of Specimens

The slump test for concrete was assessed using an Abrams cone after it had been mixed (AFNOR P 18-451). The Abrams cone slump was used to calculate handling. The new concrete was introduced into a cubic mould ($10 \times 10 \times 10$ $cm^3$) on a vibrating table for 1 min. The specimens were stored in an appropriate location for 24 h and then immersed in water according to the NFP18404 standard.

*2.4. Specimen Storage*

All of the types of specimens were kept in an appropriate area for 1 day before being submerged in water for 28 days, according to the NFP18404 standard. Following that, 4 series of test specimens were stored for 12 months in a variety of conservation environments:

- Seawater (conditions: T = 25 °C, RH 100%, pH 7–9),
- Drinking-water (conditions: T = 25 °C, RH 100%, pH 6–7),
- Open-air (conditions: T= 25 °C, RH 55%, pH 12–14),
- Oven (conditions: T = 75 °C, RH < 50%, pH 12–14).

*2.5. Experimental Methodology of Compressive Strength Test*

Each reported result for the compressive strength tests was the average of 105 samples. The seven categories of samples were tested for each series. Each kind was tested three times to ensure that the results would be reproducible. As a consequence, the total number of specimens used for each series was 21. The dry compressive strength was tested using a

Baratest AG hydraulic press built in Switzerland; the compressive strength loss (RL) and gain (RG) are computed using Formula (5):

$$RL(\%) = \left[\frac{R - R_{SC}}{R}\right] \times 100 \quad (5)$$

$R_{SC}$ is the control specimen's compressive strength (MPa), and R is the compressive strength of a specimen of the same type in each environment (MPa).

### *2.6. Density Determination*

Density was calculated by multiplying the mass of each specimen and its envelope volume, as shown in Equation (6), where $M_0$ is the weight (g), $V_0$ is the volume ($cm^3$), and is the density (g $cm^{-3}$). The average of five measurements was used to calculate the results.

$$\rho = \frac{m_0}{V_0} \quad (6)$$

### *2.7. Water Absorption Capacity Measurement*

The water absorption capacity was calculated using ASTM D 1037-12. A total of 6 specimens were submerged in water at a temperature of 20 °C for each sample. After 2 h and 24 h, the mass measurements were obtained. Each specimen's water absorption was determined as a percentage of mass gain compared to the starting mass, as shown in Equation (7) where $m_{sat}$ (g) is specimen mass in a saturated state and $m_{dry}$ (g) is the specimen mass in a dry state:

$$\omega = \left(\frac{m_{sat} - m_{dry}}{m_{dry}}\right) \quad (7)$$

### *2.8. XRD Characterization*

A Rigaku Ultima IV multipurpose X-ray diffraction apparatus was used to analyse the crystalline structure of the treated and untreated wood chips. The diffractometer was equipped with an X-ray generator (maximum rated output: 3 kW, target: Cu) and a goniometer (maximum rated output: 3 kW, target: Cu). The high score application, in accordance with the International Centre for Diffraction Data (ICDD) PDF-4, was used to identify the phases and retrieve all of the crystalline structure characteristics.

## 3. Results and Discussions

### *3.1. Ordinary Concrete*

From the findings in Figure 7, RLs of the OCs were evident in all media, and they depended on the conservation context. The compressive strength of the control OC was about 37.1 MPa. The literature shows a mean compression strength of 37.3 MPa in moulded cement composites made using Portland cement and no wood [61]. The creation of glue-water-cement explains this result during the first 28 days of concrete setting. Le Chatelier (1887) [54] described a cement hydration process based on dissolution/precipitation. When water is supplied, the anhydrous reactants will gradually dissolve. These reactants are more soluble than the products after hydration. The solution becomes supersaturated, resulting in the precipitation of hydrates. As the concentration of reactants (Table 3) falls, more ions enter the solution, allowing other hydrates to precipitate. The primary phases of Portland cement are tricalcium silicates ($C_3S$) and dicalcium silicates ($C_2S$) (Table 2). Their hydration products are hydrated calcium silicates (C-S-H) and Portlandite ($Ca(OH)_2$) [62,63].

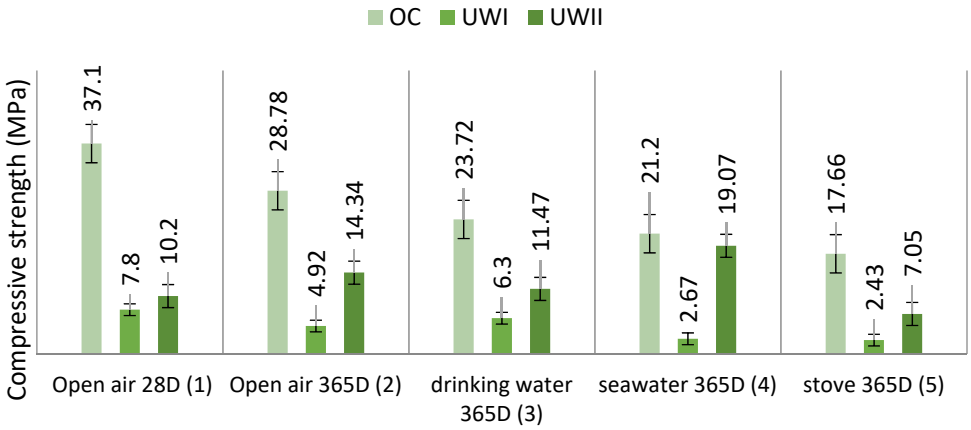


**Figure 7.** $UW_I$ and $UW_{II}$ compressive strength (in MPa) as a function of preserving media.

Figure 7 depicts RLs of 35.84%, 36.06%, 42.85%, and 52.30%, after 12 months of exposure to outdoor air, drinking water, seawater, and an oven, respectively. Hardened concrete improves its compressive strength over time under normal conditions. However, it should be noted that environmental variables, particularly RH, temperature, and inorganic salts, might influence the evolution of compressive strength.

The evaluation of the impact of RH on the compressive strength of fresh and hardened cement is based on a concerted effort and is strongly connected to the phenomena of carbonation [64]. Carbonation, according to Mahmood et al. [65], is described as a regularly diffused phenomenon in ancient reinforced concrete structures, which are typically constructed without special design requirements preventing degradation. In the carbonation process, atmospheric carbon dioxide ($CO_2$) enters the concrete cover through the capillary pores and reacts with calcium hydroxide ($Ca(OH)_2$), which is a hydration product of calcium silicate compounds present in the clinker and which is responsible for pH value reduction, resulting in the formation of calcium carbonate, as depicted by Equation (8):

$$Ca(OH)_2 + CO_2 \rightarrow CaCO_3 + H_2O \quad (8)$$

Furthermore, $CO_2$ may react with the calcium silicate hydrate (C-S-H) network to produce additional $CaCO_3$ [66]. The proportion of Portlandite ($Ca(OH)_2$) in the concrete mass determines the pH of the recycled aggregate. Because of the dissolution of $Ca(OH)_2$ and the generation of OH- in water, the pH of the recycled aggregate increases to 12 and normally ranges from 11 to 13. According to Equation (9), the presence of water in the carbonation process is required for the mobility of hydrated cement products in the pore solution and allows $CO_2$ to dissolve and create carbonic acid ($H_2CO_3$). Using the following process, this weak acid attacks Portlandite ($Ca(OH)_2$) and generates $CaCO_3$:

$$Ca(OH)_2 + H_2CO_3 \rightarrow CaCO_3 + 2H_2O \quad (9)$$

Elsalamawy et al. [67] established a direct proportionality between carbonation depth and concrete compressive strength. This is supported by Peng Liu et al. [25], who reinforced this conclusion, noting that cement type has a significant impact on concrete carbonation resistance. Metalssi et al. [67] report that, for genuine constructions exposed to natural carbonation, the concrete is saturated after demoulding and cannot be carbonated spontaneously owing to the low $CO_2$ content. Carbonation, on the other hand, might occur after a partial drying of the material, after several weeks, or even after several years (in the case of Portland cement, CEM I according to European standards) [68].

Elsalamawy et al. [67] demonstrate that RH is one of the most important elements influencing carbonation depth, with the carbonation depth increasing with increasing RH to reach a peak value at 65 percent RH, regardless of cement type. This discovery validates

the importance of the electrified RL for open-air OC preservation (conditions: RH = 65%, T = 25 °C, pH 12–14).

In addition, the same authors [67] determined relative carbonation depth by dividing the value of carbonation depth by the maximum value of carbonation depth. They established the polynomial relationship between relative carbonation depth and relative humidity (40–80%). The graph demonstrates that at RH 50%, there is insufficient moisture for carbonation to occur, and at RH > 70%, there is insufficient moisture for carbonation to occur. Therefore, it can be inferred that the carbonation phenomenon has no effect on the conservation of OC in drinking water (RH 100%), seawater (RH 100%), or the oven (RH 50%).

In drinking water and seawater, inorganic ions, such as $Cl^-$, $SO_4^{2-}$, $Mg^{2+}$, $K^+$, and $Na^+$, occur in aqueous media. According to Chen et al. [69], $Mg^{2+}$ and $SO_4^{2-}$ may be more damaging to the compressive strength of cement-based composites than other anions. The major damage caused by $SO_4^{2-}$ to concrete is crystalline corrosion [6,70], which includes the conversion of thenardite crystals to mirabilite crystals [70,71] and the volume expansion of ettringite crystals and gypsum crystals. Both of the aforementioned factors may cause a sequence of physical and chemical reactions inside the concrete, which may result in additional concrete expansion and cracking [72–74]. $Mg^{2+}$ damage is mostly indicated by the weakening of mortar and aggregate on the concrete's surface [12,75]. This is due to $Mg^{2+}$ generating magnetic $Mg(OH)_2$ inside the concrete, which has low solubility. With the continuous precipitation of Mg(OH), C-S-H cementing material degrades and produces non-cementitious M-S-H [76,77]. These considerations support the RLs obtained during OC preservation in an aqueous medium. Furthermore, due to the high concentration of mineral salt in saltwater, the RL of OC preserved in seawater is larger than that in drinking water.

Previous research on the compressive behaviour of hardened concrete at various temperatures has been conducted. As the heating temperature increased, the compressive strength of concrete with the same moisture level decreased [78]. Concrete curing temperatures below 5 °C or over 100 °C resulted in an almost 20% drop in concrete strength [79]. When the gap between the ambient and concrete temperatures was small, the mechanical performance of concrete was ideal [80]. According to El-Zohairy et al. [81], after just 90 days, concrete lost 10–20% of its initial compressive strength when heated to 100 °C and 30–40% when heated to 260 °C. Therefore, in the current study, OC maintained in the oven had the lowest compressive strength (17.66 MPa). As a result, it displayed an RL value (52.30%) that was about twice as low as that of the OC after 28 days.

### *3.2. Wood–Cement Composite*

#### 3.2.1. Untreated Redwood–Cement Concrete

Because of the nature of the untreated redwood chips, Figure 7 reveals an alarming rise in RL for all media. After 28 days, $UW_I$ was characterized by excessive water absorption and increased swelling (7.8 MPa). In general, vegetated concrete has a high porosity. Indeed, the SEM pictures of a significant variety of fibre cements in the literature exhibit several fields when compared to regular concrete [82–86]. As a result, the addition of wood fibres to concrete enhances its density. In addition, because of their porosity, these concretes are water-sensitive [87].

After 12 months of storage in the open air, 36.92%, 19.23%, and 65.76% of RLs were obtained. Wood-fibre-concrete's porous nature has a capacity to exchange moisture (or water) with the surrounding environment via the adsorption/desorption phenomena [14]. According to Mohr et al., the bulk of mechanical property losses occurred during the first five wet/dry cycles. However, ductile fibre failure was still identified using scanning electron microscopy (SEM) [88,89]. The sensitivity of vegetal concretes to humidity causes dimensional fluctuations that correspond to changes in relative humidity [90]. In addition, RH has been shown to influence at least four essential characteristics of electrospun fibres: surface morphology, interior porosity, structure, and mechanical qualities [91].

Wood-fibre–cement composites age in humid and aquatic environments, resulting in a reduction in strength and toughness. Wood composition in the specimens is often exposed to three distinct processes reducing their adherence to the matrix [41]:

- Debonding of the plant particle/matrix interfaces because of wood–water swelling.
- The degradation of plant particles is promoted by progressive alkali hydrolysis.
- Mineralization of plant particles is caused by the deposition of cement hydration products, primarily calcium hydroxide, onto the plant particle surface. On the other hand, the adhesion problem can be enhanced by modifying the particle surface.

The RL of $UW_I$ in drinking water (19.23%) is insignificant compared to the non-aqueous environments after 28 and 365 days. In addition, The RL in drinking water was about 3.5 times more than the RL of $UW_I$ stored in saltwater (65.76%). The pH of the storage media explains this finding. In fact, the pH of drinking water (pH 6) is lower than that of saltwater (pH 8–9), and the non-aqueous environments (pH 12–14). The lower the pH, the less alkaline the attack on the wood.

On the other hand, 68.84% of the RL was obtained after 12 months in the oven. Based on SEM images from the study by de Abreu Neto et al. [92], it is probable that increasing the temperature causes deformations and changes in the morphology of the wood fibres as a whole. Indeed, wood fibres exhibited a propensity for the thickness of their fibre walls to shrink with increasing temperatures. The study conducted by Dehghan et al. [93] supports this fact.

#### 3.2.2. Untreated Hardwood–Cement Concrete

Figure 7 depicts the variation of $UW_{II}$ resistance according to the storage medium. Compared to the $UW_I$ data, it is clear that the resistance improved considerably in all the selected environmental conditions. The discrepancy is explained by a difference in the absorption coefficient of the aggregates [12]. $W_I$ has a lower apparent density than $W_{II}$. However, this structure results in a material with poor strength and stiffness after cure. $W_I$ has a very high water-absorption capacity because of its porous structure, which reduces the amount of water available for the binder to set in. Furthermore, the significant migration of water via capillarity results in the movement of $Ca^{2+}$ calcium ions, which are required for binding the binder with the plant particles.

In order to verify this, the effect of the ratio of $W_I$ and $W_{II}$ on the density and adsorption capacity of $UW_I$ and $UW_{II}$ after 28 days of hardening was explored. Figure 8 demonstrates the outcomes. Figure 8a demonstrates that the densities of $UW_I$ and $UW_{II}$ reduce when the ratios of $W_I$ and $W_{II}$ in the concrete composition increase. This demonstrates that the wood chips from $W_I$ and $W_{II}$ lighten the concrete. Furthermore, Figure 8b shows that the absorption capacities of $UW_I$ and $UW_{II}$ are proportional to the rate of the wood chips. When the densities and water-absorption capacities of the two concretes are compared, it is evident that the densities and water-absorption capacities of $UW_{II}$ are greater than those of $UW_I$. This demonstrates that $W_I$ has a lower density and a higher water-absorption capacity than $W_{II}$.

According to Mukhopadhyay et al. [94], the degrees of deterioration caused by an alkaline environment attack on the vegetal additive's composition vary. The loss of mechanical characteristics of various vegetables additives' composition determines the extent of the damage. The severity of the attack ranges from a severe loss of strength to almost no loss of strength. It is governed by the capacity of the vegetal additive's composition to absorb water.

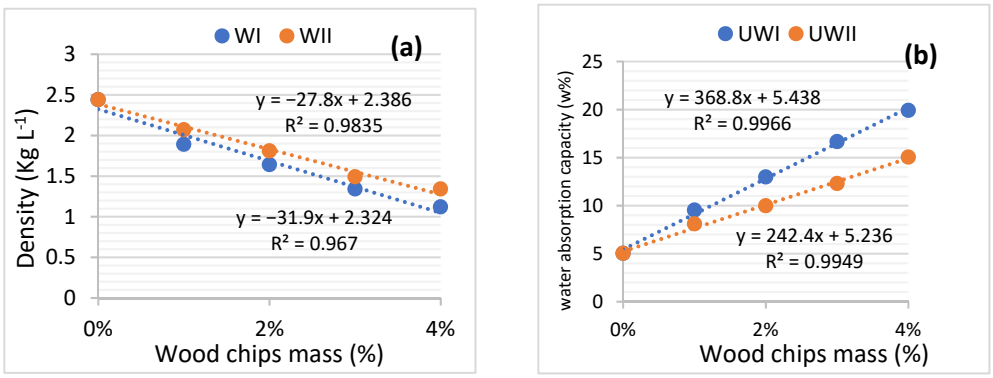


**Figure 8.** $UW_I$ and $UW_{II}$ (**a**) water-absorption capacity, and (**b**) density in function of wood chips' mass.

The RG in all sectors, on the other hand, is lower than the OC. The result was that 15.67, 28.42, and 86.96% of RG were allocated when the $UW_{II}$ samples were in the open air, potable water, and seawater. However, soaking $UW_{II}$ in saltwater for 12 months yielded the best compressive strength results. Indeed, $UW_{II}$ increased in its compressive strength by 40.5%. Even though multiple investigations have yielded equivalent results [72], the behaviour of concrete loaded with wood augmentation methods in saline solutions is still poorly understood. The rise in its compressive strength in seawater is due to the high concentration of inorganic salts. The concentration of inorganic ions in saltwater is greater than that in drinking water [95,96]. However, the competition for $OH^-$ and $Ca^{2+}$ attachment to the surface of wood chips with other inorganic ions is more crucial.

### *3.3. Treated Wood-Containing Concrete*

#### 3.3.1. Cement Treatment of Wood

To improve some of the properties of the investigated compositions, such as water sensitivity and wood–matrix adhesion, treating the wood pieces before incorporating them into the concrete was considered. Various treatments have been used in previous works, and it has been demonstrated that coating with cement produces satisfactory results, particularly in terms of compressive strength. Because of this impact, $W_I$ and $W_{II}$ were treated with cement before being included in the concrete mixture. Figure 9 depicts the findings of the compressive strength of $TW_{IC}$ and $TW_{IIc}$, respectively, preserved in different media. The shaving treatment significantly enhanced the compressive strength of $TW_{IC}$ and $TW_{IIc}$ in all tested media, resulting in a suitably light structural weight. These findings are consistent with Bedirinan's study [28].

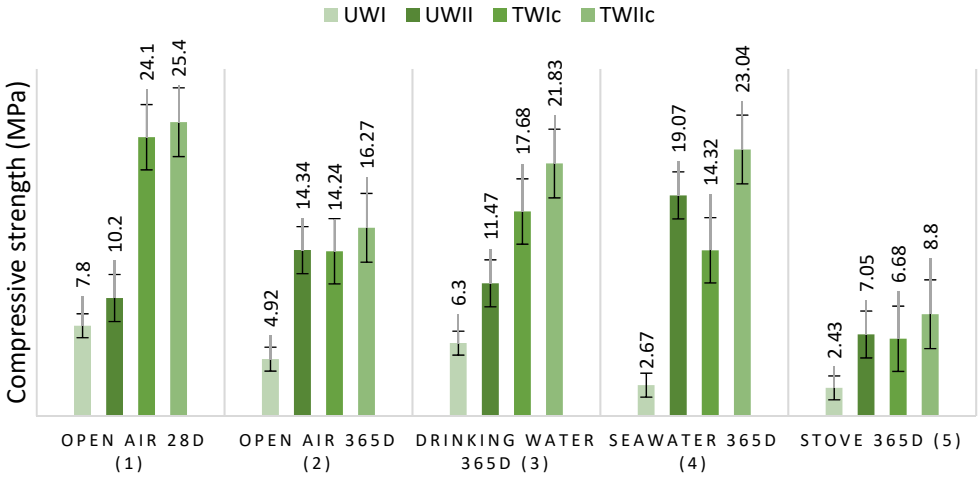


**Figure 9.** $UW_I$, $UW_{II}$, $TW_{IC}$, and $TW_{IIC}$ compressive strengths as a function of preserving media.

Wood treatment lowers the porosity of $TW_{IC}$ and $TW_{IIC}$ structures, increasing the composites densities and decreasing the water capacities. This perspective is supported by Figure 10. It shows the findings of the change in the density and water absorption capacity of $TW_{Ic}$ and $TW_{IIc}$ as a function of the mass of $W_I$ and $W_{II}$ treated with cement and lime. When the equations of Figures 8a and 10a are compared, the tangents of the density plots of $TW_{IC}$ and $TW_{IIC}$ are higher than those of $UW_I$ and $UW_{II}$. Similarly, the tangents of the water-absorption capacity graphs of $TW_{IC}$ and $TW_{IIC}$ are lower than those of $U_{WI}$ and $U_{WII}$ (Figures 8b and 10b). These are the results of the wood-chip treatment. This finding demonstrates that treating wood chips with cement is an efficient way to create a more durable wood–cement composite.

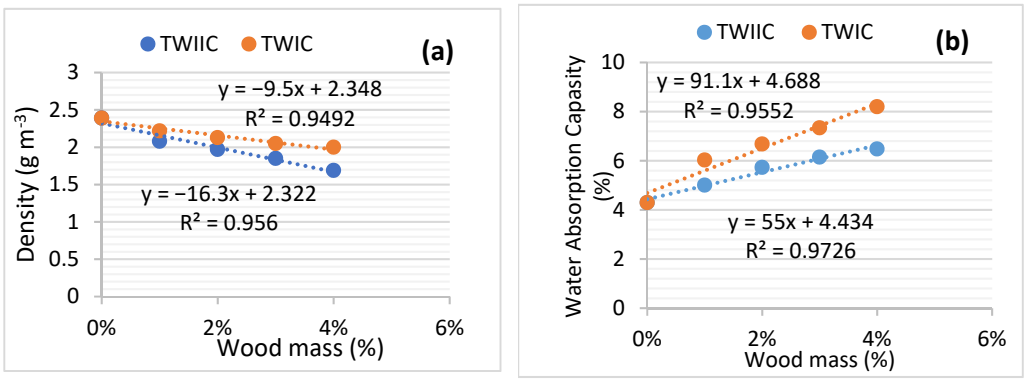


**Figure 10.** $TW_{Ic}$ and $TW_{IIc}$: (**a**) density, and (**b**) water-absorption capacity as a function of wood-chip mass.

In addition, it improves wood–matrix adhesion since the coating of the chips in a layer of cement is likely to reinforce the adhesion with the cementitious matrix. It is possible that the pre-coating of the chips minimizes the hygroscopic effect and increases the wood–matrix adhesion. The images of the SEM of treated and untreated wood chips ($W_I$ and $W_{II}$) in Figure 11 indicated that the cement matrix takes the shape of plates, and the distribution is random. They are more frequent in less inhabited places and specimens made of cement-treated chips. They can be seen clearly on the surface of the treated chips and do not exist on the untreated chips. These findings support the notion that the adhesion between wood and cement is poor. Furthermore, if the cement concentration in the treatment product is high, the paste layer coating the wood grains may be thicker, resulting in higher wood rigidity [72]. Consequently, significant compressive strength is attained in all of the investigated media.

### 3.3.2. Mechanism of Cement–Wood Treatment

Based on Table 2, it is possible to conclude that the cement was constituted chiefly of lime (60.41%). Given this fact, $W_I$ and $W_{II}$ were subjected to lime treatment to understand better the influence of cement treatment chemistry on compressive strength. Figure 12 shows the results of $TW_{IL}$ and $TW_{IIL}$ compression strength in relation to the conservation medium. Figure 13 shows that $TW_{IL}$ and $TW_{IIL}$ were less resistive after 28 days than were $TW_{IC}$ and $TW_{IIC}$. The compression strengths of $TW_{IL}$ and $TW_{IIL}$ were 14.60 MPa and 15.05 MPa, respectively. The findings indicate that the strength of the concrete is only affected by the cement's composition after 28 days in open air.

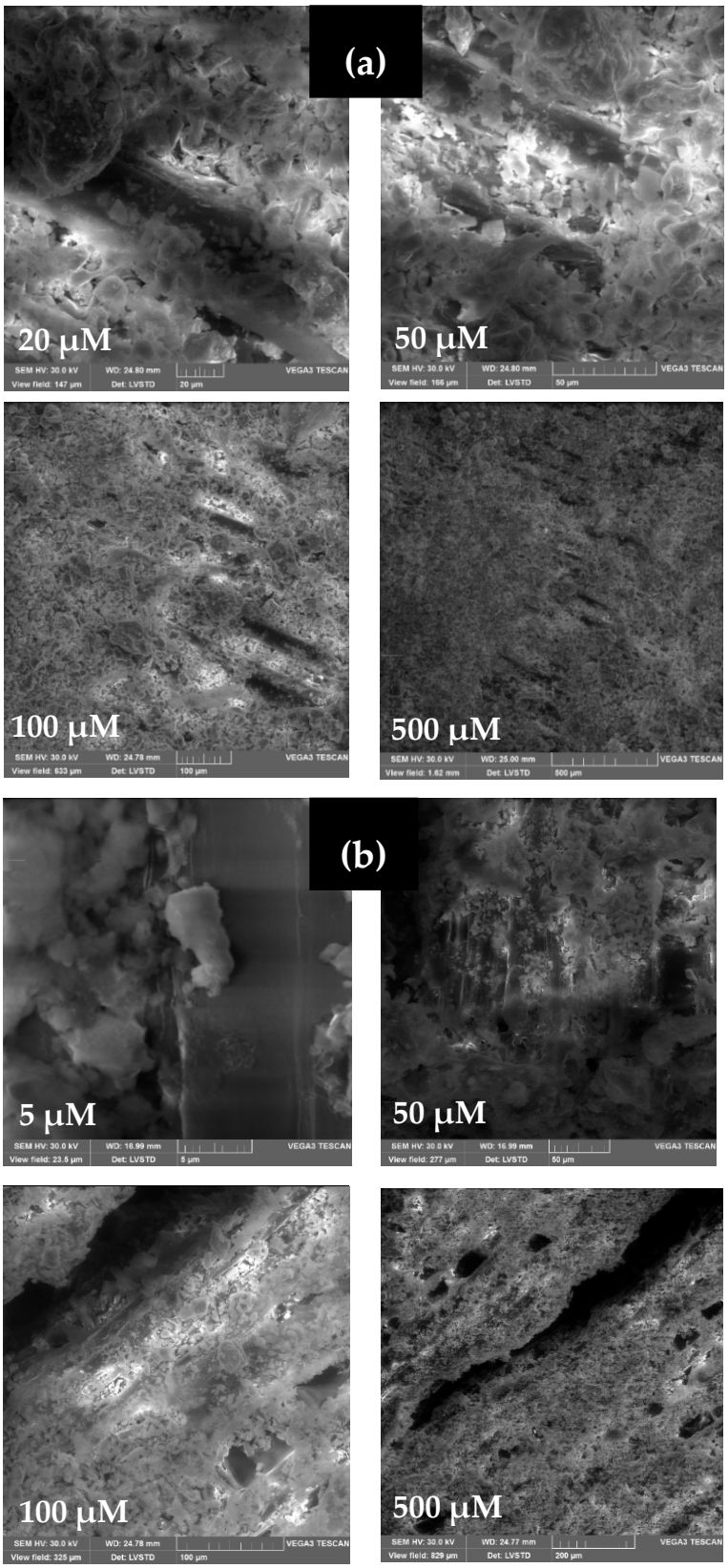


**Figure 11.** SEM microstructural images of (**a**) $W_{IC}$ and (**b**) $W_{IIC}$.

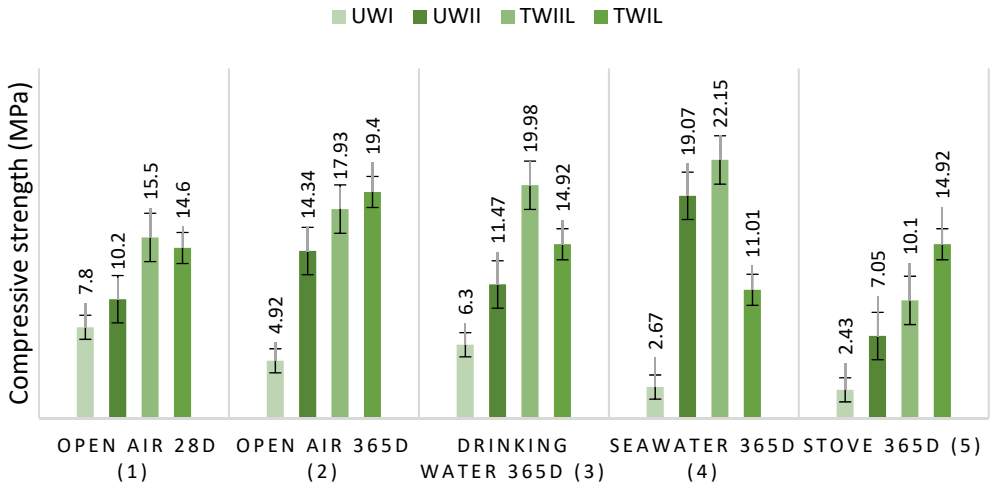


**Figure 12.** $UW_I$, $UW_{II}$, $TW_{IL}$, and $TW_{IIL}$ compressive strength as a function of preserving media.

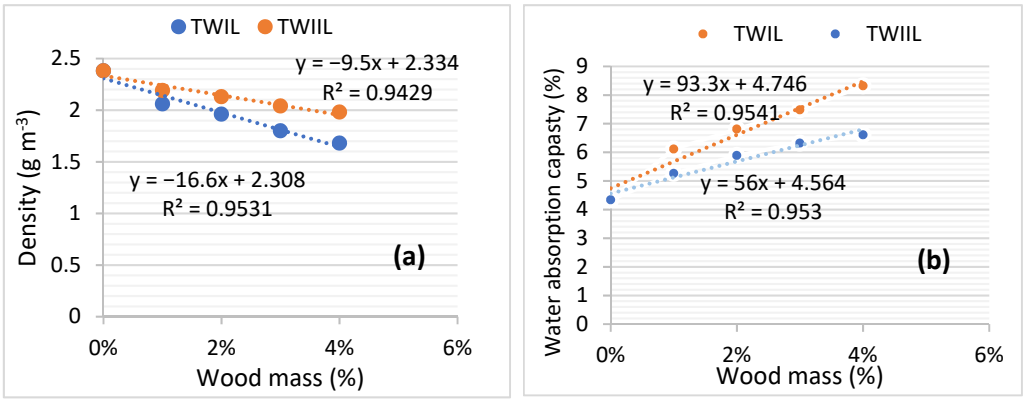


**Figure 13.** $TW_{IL}$ and $TW_{IIL}$ (**a**) density, and (**b**) water-absorption capacity as a function of wood-chip mass.

Figure 12 shows clear improvements in the specimens' compression strength after 365 days of conservation in all environments investigated. This finding is supported by the fact that both $TW_{IL}$ and $TW_{IL}$ resistances were improved by 8.5 MPa compared to $UW_I$ and $UW_{II}$ resistances. The enhanced resistance was due to the lime's ability to act as a surface layer for the wood chips [97]. This finding indicates that the improvement in compression strength of the $TW_{IC}$ and $TW_{IIC}$ was primarily attributable to the lime.

Figure 13 shows the findings regarding $TW_{IL}$ and $TW_{IIL}$ density and water-absorption capacity in relation to the mass of the wood chips. The tangents of the density plots of $TW_{IL}$ compared to $TW_{Ic}$, as well as $TW_{IIL}$ compared to $TW_{IIC}$, are almost identical. This means that the lime in the cement maintains the impermeability of water in the wood. However, $TW_{IL}$ acquired resistance in all of the storage media except saltwater according to Table 7 (−24.59%). Similarly, besides the oven (−30.88%), all conservation zones in $TW_{IIL}$ exhibited a grain in strength. The LRs collected are not related to the $W_{IL}$ and $W_{IIL}$ lime treatments.

**Table 7.** RL/RG of $TW_{IIL}$ and $TW_{IIL}$ as a function of preserving media.

| Environment | $TW_{IL}$ | $TW_{IIL}$ |
|---|---|---|
| 28 days | 0 | 0 |
| Open air | 32.88 | 40.59 |
| Drinking Water | 2.19 | 12.45 |
| Seawater | −24.59 | 86.96 |
| Oven | 2.19 | −30.88 |

The XRD patterns of $W_{II}$, $W_{IIc}$, and $W_{IIL}$ are shown in Figure 14. Tables 8 and 9 present structural characteristics derived from XRD characterizations of $W_I$ and $W_{II}$, respectively.

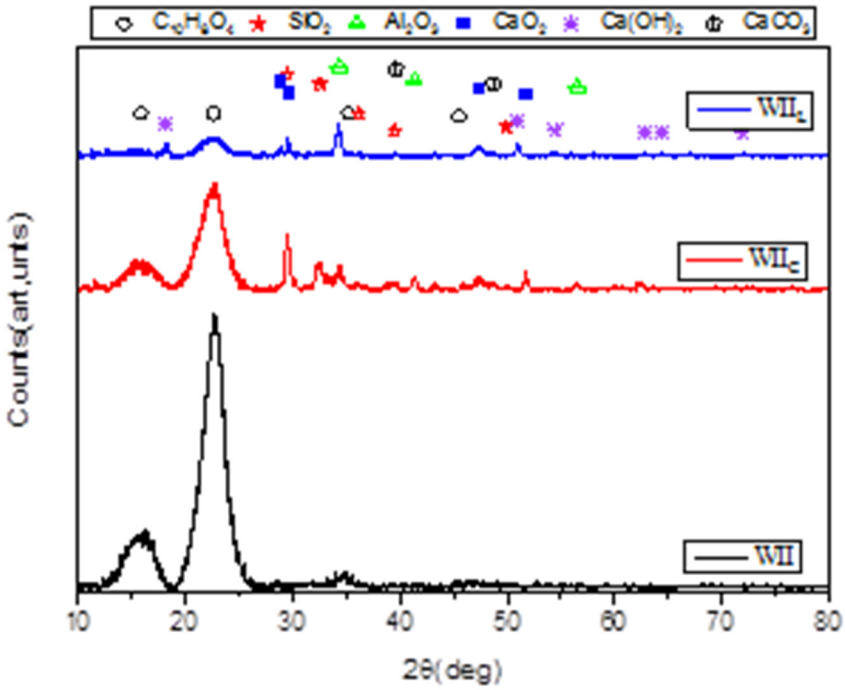


**Figure 14.** XRD spectra of $W_{II}$, $W_{IIc}$, and $WI_{IL}$ samples.

**Table 8.** Structural parameters obtained from XRD characterizations of $W_I$, $W_{Ic}$, $W_{IL}$.

| Wood Samples | Chemical Structure | JCPDS Card No | D (nm) | | ε (μm) |
|---|---|---|---|---|---|
| | | | Scherrer Method | W–H Method | |
| $W_I$ | $C_{10}H_8O_4$ | 27-1905 | 1.83 | 1.30 | $5.73 \times 10^{-2}$ |
| | $Al_2O_3$ | 42-1468 | | | |
| $W_{IC}$ | $SiO_2$ | 82-1232 | 21.55 | 8.40 | $5.60 \times 10^{-4}$ |
| | $CaO_2$ | 03-0865 | | | |
| | $CaCO_3$ | 01-0837 | | | |
| $W_{IL}$ | $Ca(OH)_2$ | 89-2779 | 11.83 | 7.55 | $6.43 \times 10^{-4}$ |
| | $CaO_2$ | 85-0514 | | | |

***D**: Crystallite size (nm), **W–H**: Williamson-Hall, **ε**: Micro-strain.*

**Table 9.** Structural parameters obtained from XDR characterizations of $W_{II}$, $W_{IIc}$, $W_{IIL}$.

| Wood Samples | Chemical Structure | JCPDS Card No | D (nm) | | ε (μm) |
|---|---|---|---|---|---|
| | | | Scherrer Method | W–H Method | |
| $W_{II}$ | $C_{10}H_8O_4$ | 27-1905 | 1.83 | 1.30 | $5.73 \times 10^{-2}$ |
| | $Al_2O_3$ | 42-1468 | | | |
| $W_{IIC}$ | $SiO_2$ | 82-1232 | 8.168 | 1.82 | $9.36 \times 10^{-3}$ |
| | $CaO_2$ | 03-0865 | | | |
| | $CaCO_3$ | 01-0837 | | | |
| $W_{IIL}$ | $Ca(OH)_2$ | 89-2779 | 15.77 | 8.34 | $5.15 \times 10^{-4}$ |
| | $CaO_2$ | 85-0514 | | | |

***D**: Crystallite size (nm), **W–H**: Williamson–Hall, **ε**: Micro-strain.*

The XRD data for $W_I$ and $W_{II}$ (Tables 8 and 9) revealed 4 major peaks at 15.85°, 22.60°, 35.19°, and 45.49°. Those peaks could be attributable to $C_{10}H_8O_4$ (27-1905), a derivative

of cellulose crystal planes ($C_6H_{10}O_4$) in wood fibres ($W_I$ and $W_{II}$) [98,99]. Thus, according to Camargo et al. [41], the major component of plant fibres is cellulose. In addition, no typical peaks at 16.85° and 22.60° were detected, as shown in Figure 14. A previous study of bamboo surfaces, investigated by Bao et al. [100], supports this fact. On the other hand, the XRD data of cement-treated wood ($W_{IC}$ and $W_{IIC}$), are differentiated by 3 peak ranges, namely: (i) 5 peaks at 47.32°, 48.62°, 51.74°,and 62.32° attribute to $CaO_2$ (03-0865), which is derived from lime crystal (CaO) [5]; (ii) 7 peaks at 22.43°, 29.46°, 32.54°, 36.18°, 38.78°, 39.46°, and 49.90° attribute to $SiO_2$ (82-1232); (iii) and 3 peaks at 34.34°, 41.35°, 43.53°, and 56.56° attribute to $Al_2O_3$ (42-1468).

In comparison to Tables 2 and 3, the elements of cement with the largest weight percentages are CaO, $SiO_2$, and $Al_2O_3$, in that order. They are also prominent components of clinkers, with $FeO_2$, in low proportion, being the most abundant. This allows us to state that the cement has attached to the surface of the wood because the clinkers act as a glue. [101]. Similarly, there are 3 distinct sets of peaks in the lime-treated wood ($W_{IL}$ and $W_{IIL}$) spectra, namely: (i) 4 peaks at 28.84°, 29.58°, and 84.92° attribute to $CaO_2$ (85-0514), (ii) 8 peaks at 18,19°, 34.25°, 47.33°, 50.94°, 54.49°, 62.76°, 64.49°, and 71.92° attribute to $Ca(OH)_2$ (89-2779); and (iii) 4 peaks at 22.53°, 39.59°, 43.30°, and 48.68° attribute to $CaCO_3$ (01-0837).

Based on these findings, it is possible to deduce that the adherence of the lime on the surface of the wood is only made by $Ca(OH)_2$. The existence of $CaCO_3$ on the surface of the wood is supported by the attack on $Ca(OH)_2$ by humidity and $CO_2$ in the air. According to Okayinkwa et al. [102], calcium carbonate significantly boosts the compressive strength of wood–cement concrete by decreasing its permeability. Furthermore, an SEM image of $CaCO_3$/Wood–concrete, investigated by Merk et al. [103], shows that $CaCO_3$ may be introduced deep into the wood structure using alternating solution–exchange cycles of extremely concentrated electrolytes $NaHCO_3$ in water. Despite this fact, in the work conducted by Mejri et al. [104], it was demonstrated that the presence of sulphate and magnesium ions lowered the crystal development rate and decreased the quantity of $CaCO_3$ precipitates obtained at a constant temperature and ionic strength. Magnesium caused the production of aragonite rather than calcite or vaterite. The presence of magnesium and sulphate ions caused changes in the effect of magnesium on the kinetics of $CaCO_3$ precipitation, resulting in the incorporation of $Mg^{2+}$ ions in the $CaCO_3$ lattice. This explains the RL for $TW_{IL}$ obtained after 365 days in sea water (Table 7).

On the other hand, according to Cheng Bencedira et al. [105], the increase in temperature increases $CaCO_3$ precipitation in water (RH 100%). However, the $CaCO_3$ precipitation depends on the percentage of RH in the medium. Indeed, according to Pondelak et al. [106], After one year of exposure at RH 33% and T = 45 °C, the $CaCO_3$ does not precipitate. As a consequence, $TW_{IL}$ loses 30.88% of its compression resistance. It is hypothesized that $CaCO_3$'s stability is owing to the restricted quantity of water physiosorbed on the surface of the wood fibres, which is thought to be the driving factor for its precipitation.

According to Graine et al. [107], the average diameter of treated/untreated samples is calculated by measuring the width at half-height of the respective XRD peaks and by employing two methods, Scherrer's and Williamson–Hall. Scherrer's principle indicates that the widening of the XRD peaks is solely attributable to particle size. Using Equation (10), we can calculate the average crystallite size from the X-ray patterns:

$$D = \frac{K\lambda}{\beta_{corrected}\ cos\theta} \tag{10}$$

where $D$ is the mean crystallite size, $K$ is the crystallite form factor (12), is the X-ray wavelength, corrected is the full width at half the maximum of the peak, and is the diffraction angle. For correct calculations, the instrumental broadening effect and the observed XRD

pattern peaks must be separated. As a result, Equation (11) can be used to estimate the corrected broadening, which is simply influenced by particle size.

$$\beta_{corrected}\ cos\theta = (\beta_{obseved}\ - \beta_{unstrumental})^{\frac{1}{2}} \quad (11)$$

However, the broadening of the XRD peaks might also be attributable to the lattice's micro-strain impact. As a result, for greater precision, we must also separate the crystallite size effect and the micro-strain impact. In this paper, the Williamson–Hall approach was employed, which assumes Equation (12) where is $\varepsilon$ is the micro-strain in the lattice:

$$\beta_{corrected} cos\theta = 4\varepsilon sin\theta + \frac{K\lambda}{D} \quad (12)$$

$D$ variation is shown in Table 7 as 1.30 nm, 8.40 nm, and 7.55 nm by the Scherrer technique, and 1.83 nm, 21.55 nm, and 11.83 nm by the Scherrer method for $W_I$, $W_{Ic}$, and $W_{IL}$, respectively, while, the variation of $D$ for $W_{II}$, $W_{IIc}$, and $W_{IIL}$ (Table 9) is 1.30 nm, 1.82 nm, and 8.34, respectively, according to the Williamson–Hall approach (Figure 15a) and 1.30 nm, 8.16nm, and 15.77 nm, respectively, according to the Scherrer method (Figure 15b). These data indicate that the wood chips' Ds before treatment are the same. This supports the wood chip diameter results using granulometric analysis. In addition, the two approaches' calculations demonstrate that the diameter of the wood particles increases when they are treated. In fact, $D$ of cement-treated wood is larger than $D$ of lime-treated particles. As a result, when the wood surfaces are treated, the lattice strain decreases. Indeed, the best lattice strain findings are attributable to $W_{IC}$ and $W_{IIC}$. The reduction in lattice strain is reflected in the reduction in spacing within the minimum wood width. As a result, the density of the wood rises, while its capacity to absorb water diminishes. The study conducted by Zhang et al. [108] supports this argument.

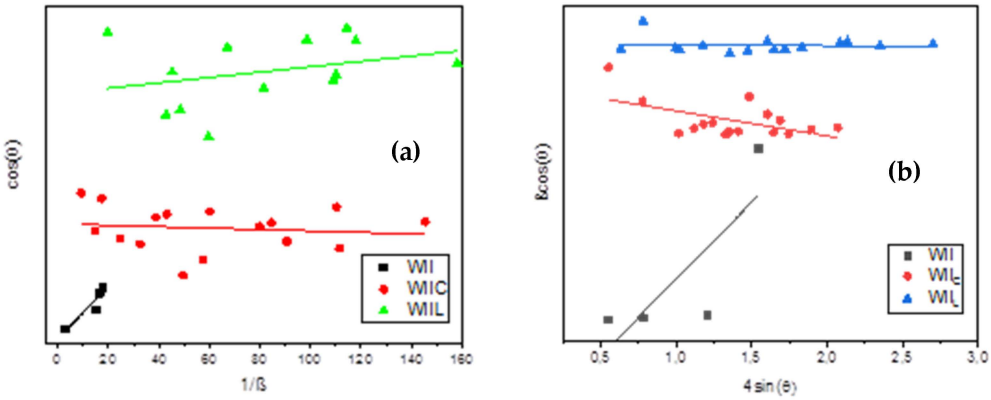


**Figure 15.** Particle size determination from (**a**) Scherrer's and (**b**) Williamson–Hall plots derived from X-ray data for $W_{II.}$

## 4. Conclusions and Limitations

This work contributes to the broader challenge of sustainable development by improving wood–concrete composites' physical characteristics to expand their range of use. As a result, this work aimed to investigate the influence of various environments on the compression strength of concrete containing hardwood or redwood shavings. The studied storage environments were: open-air (T = 25 °C, RH 55%, pH 12–14), drinking water (T = 25 °C, RH 100%, pH 6–7), seawater (T = 25 °C, RH 100%, pH 7–9) and an oven (T = 75 °C, RH < 50%, pH 12–14). Due to the complex mechanisms involved in this study, only the compressive strength was experimentally measured. The main findings obtained are:

- Ordinary concrete strength diminishes after 365 days of storage in every medium investigated compared to its strength after 28 days. Depending on the environment studied, this decrease is significant.
- In all conditions investigated, the addition of wood (redwood or hardwood) to the concrete reduces its resistance. The low mechanical resistance of vegetable concretes is partly due to the high water-absorption of wood chips and the poor wood–matrix adhesion.
- Concrete made of untreated hardwood is more resistant, in all preservation media, than concrete made of redwood due to its high apparent density.
- Seawater enhances the strength of hardwood-based concrete. Indeed, compressive strength results for ordinary concrete and hardwood-based concrete are comparable.
- The treatment of wood enhances the compressive strength after 365 days in all conservation media. The lime in cement acts on wood chips by (i) coating the surface of the wood, which lowers the porosity subtract of wood-based concrete, (ii) and reinforces the wood–matrix adhesion. The other cement constituents are only involved during the curing step (the first 28 days).

Even though treating wood with cement coating improves its resistance in watery environments, its resistance in dry and wet environments remains lower. The resistance of OC surpasses that of $TW_{IIc}$ by 11.7 MPa, 12.51 MPa, and 8.86 MPa, respectively, after 28 days in the open air and 365 days in the open air and the oven. However, OC and $TW_{IIC}$ resistance after 365 days in drinking water and saltwater are comparable. This enables us to conclude that the efficiency of cement treatment of wood for boosting compressive strength is restricted solely to watery conservation conditions. The research has implications for academics where the results of the study can be used to understand the wood–concrete composite material further. Some of the remedies to enhance its performance can include (a) describing the failure mode of each series using a variety of analytic methods, (b) changing the treatment of the surface of wood chips to linseed oil, (c) changing the type of surface treated, or (d) combining two forms of therapies.

**Author Contributions:** Conceptualization, W.K. and S.B.; methodology, S.B., M.A. (Marc Azab) and M.S.R.; software, S.B.; validation, H.A.A., M.A. (Marc Azab), M.S.R. and A.E.K.; formal analysis, S.B., M.A. (Marc Azab), M.S.R., M.A. (Mirvat Abdallah) and Z.A.B.; investigation, W.K.; resources, S.B.; data curation, M.A. (Marc Azab), M.S.R., M.A. (Mirvat Abdallah) and Z.A.B.; writing—original draft preparation, W.K. and S.B.; writing—review and editing, S.B., H.A.A., M.A. (Marc Azab), M.S.R., M.A. (Mirvat Abdallah) and Z.A.B.; visualization, H.A.A.; supervision, M.S.R. and A.E.K.; project administration, S.B.; funding acquisition, M.A. (Marc Azab), M.S.R., M.A. (Mirvat Abdallah) and Z.A.B. All authors have read and agreed to the published version of the manuscript.

**Funding:** This study was supported by the DGRSDT and the MESRS.

**Institutional Review Board Statement:** Not applicable.

**Informed Consent Statement:** Not applicable.

**Data Availability Statement:** The data presented in this study are available upon request from the corresponding author.

**Acknowledgments:** Andrey E. Krauklis' contribution was funded by the European Regional Development Fund within the Activity 1.1.1.2, "Post-doctoral Research Aid", of the Specific Aid Objective 1.1.1 of the Operational Programme "Growth and Employment" (Nr.1.1.1.2/VIAA/4/20/606). Considerable appreciation is addressed to the DGRSDT (Directorate-General of Scientific Research and Technological Development of Algeria) and the MESRS (Ministry of Higher Education and Scientific Research of Algeria) for their valuable support. Many thanks are addressed to Graine R. for his valuable help with the laboratory experiments.

**Conflicts of Interest:** The authors declare no conflict of interest.

## References


1. Woo, Y.-E.; Cho, G.-H. Impact of the Surrounding Built Environment on Energy Consumption in Mixed-Use Building. *Sustainability* **2018**, *10*, 832. [CrossRef]
2. Santamouris, M.; Vasilakopoulou, K. Present and Future Energy Consumption of Buildings: Challenges and Opportunities towards Decarbonisation. *E-Prime* **2021**, *1*, 100002. [CrossRef]
3. Haddad, S.; Barker, A.; Yang, J.; Kumar, D.I.M.; Garshasbi, S.; Paolini, R.; Santamouris, M. On the Potential of Building Adaptation Measures to Counterbalance the Impact of Climatic Change in the Tropics. *Energy Build.* **2020**, *229*, 110494. [CrossRef]
4. Andrew, R.M. Global $CO_2$ emissions from cement production. *Earth Syst. Sci. Data* **2018**, *10*, 195–217. [CrossRef]
5. Immonen, K.; Lyytikäinen, J.; Keränen, J.; Eiroma, K.; Suhonen, M.; Vikman, M.; Leminen, V.; Välimäki, M.; Hakola, L. Potential of Commercial Wood-Based Materials as PCB Substrate. *Materials* **2022**, *15*, 2679. [CrossRef] [PubMed]
6. Tariq, H.; Siddique, R.M.A.; Shah, S.A.R.; Azab, M.; Attiq-Ur-Rehman; Qadeer, R.; Ullah, M.K.; Iqbal, F. Mechanical Performance of Polymeric ARGF-Based Fly Ash-Concrete Composites: A Study for Eco-Friendly Circular Economy Application. *Polymers* **2022**, *14*, 1774. [CrossRef] [PubMed]
7. Ghafoor, S.; Hameed, A.; Shah, S.A.R.; Azab, M.; Faheem, H.; Nawaz, M.F.; Iqbal, F. Development of Construction Material Using Wastewater: An Application of Circular Economy for Mass Production of Bricks. *Materials* **2022**, *15*, 2256. [CrossRef]
8. Implementing Sustainable Development in the Construction Industry: Constructors' Perspectives in the US and Korea-Son-2011-Sustainable Development-Wiley Online Library. Available online: https://onlinelibrary.wiley.com/doi/10.1002/sd.442 (accessed on 7 April 2022).
9. Kumar, P.R.; Sreelekshmi, K.S.; Babu Anjana, S.; Harikrishnan, S.; Nath Santhanu, G.; Leena, V.P. Role of Agricultural Wastes in Construction Industry. *Int. J. Eng. Res.* **2020**, *9*, 66–69. [CrossRef]
10. Wi, K.; Lee, H.-S.; Lim, S.; Song, H.; Hussin, M.W.; Ismail, M.A. Use of an Agricultural By-Product, Nano Sized Palm Oil Fuel Ash as a Supplementary Cementitious Material. *Constr. Build. Mater.* **2018**, *183*, 139–149. [CrossRef]
11. Maraveas, C. Production of Sustainable Construction Materials Using Agro-Wastes. *Materials* **2020**, *13*, 262. [CrossRef]
12. He, J.; Kawasaki, S.; Achal, V. The Utilization of Agricultural Waste as Agro-Cement in Concrete: A Review. *Sustainability* **2020**, *12*, 6971. [CrossRef]
13. Mayer-Laigle, C.; Ibarra, L.H.; Breysse, A.; Palumbo, M.; Mabille, F.; Palacio, A.M.L.; Barron, C. Preserving the Cellular Tissue Structure of Maize Pith Though Dry Fractionation Processes: A Key Point to Use as Insulating Agro-Materials. *Materials* **2021**, *14*, 5350. [CrossRef] [PubMed]
14. Madrid, M.; Orbe, A.; Rojí, E.; Cuadrado, J. The Effects of By-Products Incorporated in Low-Strength Concrete for Concrete Masonry Units. *Constr. Build. Mater.* **2017**, *153*, 117–128. [CrossRef]
15. Figaredo, A.T.; Dhanya, M. Development of Sustainable Brick Materials Incorporating Agro-Wastes: An Overview. *Development* **2018**, *5*, 721–726.
16. Helepciuc (Gradinaru), C.M.; Barbuta, M.; Serbanoiu, A.A. Characterization of a Lightweight Concrete with Sunflower Aggregates. *Procedia Manuf.* **2018**, *22*, 154–159. [CrossRef]
17. Ledhem, A. Contribution à l'étude d'un Béton de Bois. Mise Au Point d'un Procédé de Minimisation Des Variations Dimensionnelles d'un Composite Argile-Ciment-Bois. Doctoral Dissertation, INSA, Lyon, France, 1997.
18. Singh, H.; Gupta, R. Influence of Cellulose Fiber Addition on Self-Healing and Water Permeability of Concrete. *Case Stud. Constr. Mater.* **2020**, *12*, e00324. [CrossRef]
19. Jamshaid, H.; Mishra, R.K.; Raza, A.; Hussain, U.; Rahman, M.L.; Nazari, S.; Chandan, V.; Muller, M.; Choteborsky, R. Natural Cellulosic Fiber Reinforced Concrete: Influence of Fiber Type and Loading Percentage on Mechanical and Water Absorption Performance. *Materials* **2022**, *15*, 874. [CrossRef]
20. Sajjala, K. A Review on Natural Fibres in the Concrete. *Int. J. Adv. Technol. Eng. Explor.* **2017**, *1*, 32–35.
21. Liu, J.; Lv, C. Research Progress on Durability of Cellulose Fiber-Reinforced Cement-Based Composites. *Int. J. Polym. Sci.* **2021**, *2021*, 1014531. [CrossRef]
22. Janne Pauline, S.N.; Michael Angelo, B.P. Development of Abaca Fiber-Reinforced Foamed Fly Ash Geopolymer. *MATEC Web Conf.* **2018**, *156*, 05018. [CrossRef]
23. Younes, M.M.; Abdel-Rahman, H.A.; Khattab, M.M. Utilization of Rice Husk Ash and Waste Glass in the Production of Ternary Blended Cement Mortar Composites. *J. Build. Eng.* **2018**, *20*, 42–50. [CrossRef]
24. Zareei, S.A.; Ameri, F.; Bahrami, N. Microstructure, Strength, and Durability of Eco-Friendly Concretes Containing Sugarcane Bagasse Ash. *Constr. Build. Mater.* **2018**, *184*, 258–268. [CrossRef]
25. Sanjay, M.R.; Madhu, P.; Jawaid, M.; Senthamaraikannan, P.; Senthil, S.; Pradeep, S. Characterization and Properties of Natural Fiber Polymer Composites: A Comprehensive Review. *J. Clean. Prod.* **2018**, *172*, 566–581. [CrossRef]
26. Liu, J.; Lv, C. Durability of Cellulosic-Fiber-Reinforced Geopolymers: A Review. *Molecules* **2022**, *27*, 796. [CrossRef] [PubMed]
27. Mayer, A.K.; Kuqo, A.; Koddenberg, T.; Mai, C. Seagrass- and Wood-Based Cement Boards: A Comparative Study in Terms of Physico-Mechanical and Structural Properties. *Compos. Part Appl. Sci. Manuf.* **2022**, *156*, 106864. [CrossRef]
28. Bederina, M.; Laidoudi, B.; Goullieux, A.; Khenfer, M.M.; Bali, A.; Quéneudec, M. Effect of the Treatment of Wood Shavings on the Physico-Mechanical Characteristics of Wood Sand Concretes. *Constr. Build. Mater.* **2009**, *23*, 1311–1315. [CrossRef]
29. Koohestani, B.; Koubaa, A.; Belem, T.; Bussière, B.; Bouzahzah, H. Experimental Investigation of Mechanical and Microstructural Properties of Cemented Paste Backfill Containing Maple-Wood Filler. *Constr. Build. Mater.* **2016**, *121*, 222–228. [CrossRef]

30. Anh, L.D.H.; Pásztory, Z. An Overview of Factors Influencing Thermal Conductivity of Building Insulation Materials. *J. Build. Eng.* **2021**, *44*, 102604. [CrossRef]
31. Li, M.; Khelifa, M.; Ganaoui, M.E. Mechanical Characterization of Concrete Containing Wood Shavings as Aggregates. *Int. J. Sustain. Built Environ.* **2017**, *6*, 587–596. [CrossRef]
32. Mathis, D.; Blanchet, P.; Lagière, P.; Landry, V. Performance of Wood-Based Panels Integrated with a Bio-Based Phase Change Material: A Full-Scale Experiment in a Cold Climate with Timber-Frame Huts. *Energies* **2018**, *11*, 3093. [CrossRef]
33. Fadhel, A.; Sabrine, A. Preparation and Evaluation of the Influence of Modified Fiber Flour Wood on the Properties of the Fresh Condition of Cement-Based Mortars. *Int. J. Ind. Chem.* **2018**, *9*, 265–276. [CrossRef]
34. Yang, X.; Tang, X.; Ma, L.; Sun, Y. Sound Insulation Performance of Structural Wood Wall Integrated with Wood Plastic Composite. *J. Bioresour. Bioprod.* **2019**, *4*, 111–118. [CrossRef]
35. Ribeiro, R.S.; de Sousa, R.P.; Amarilla, R.S.D.; Sant'Ana, L.H.; Avelar, M.; Catai, R.E.; Matoski, A. Sound Insulation of a Hollow Concrete Blocks Wall Made with Construction and Demolition Waste and Wood-Based Panels as Linings. *Build. Acoust.* **2021**, *28*, 423–442. [CrossRef]
36. GUNDUZ, L.; KALKAN, S.O.; ISKER, A.M. Effects of Using Cement-Bonded Particle Boards with a Composite Component in Terms of Acoustic Performance in Outdoor Noise Barriers. *Eurasia Proc. Sci. Technol. Eng. Math.* **2018**, *4*, 246–255.
37. Sarı, A.; Hekimoğlu, G.; Tyagi, V.V. Low Cost and Eco-Friendly Wood Fiber-Based Composite Phase Change Material: Development, Characterization and Lab-Scale Thermoregulation Performance for Thermal Energy Storage. *Energy* **2020**, *195*, 116983. [CrossRef]
38. Petrella, A.; Gisi, S.D.; Clemente, M.E.D.; Todaro, F.; Ayr, U.; Liuzzi, S.; Dobiszewska, M.; Notarnicola, M. Experimental Investigation on Environmentally Sustainable Cement Composites Based on Wheat Straw and Perlite. *Materials* **2022**, *15*, 453. [CrossRef] [PubMed]
39. Usman, M.; Khan, A.Y.; Farooq, S.H.; Hanif, A.; Tang, S.; Khushnood, R.A.; Rizwan, S.A. Eco-Friendly Self-Compacting Cement Pastes Incorporating Wood Waste as Cement Replacement: A Feasibility Study. *J. Clean. Prod.* **2018**, *190*, 679–688. [CrossRef]
40. ALmusawi, A.M.; ALzaidi, Z.A.; Qasim, T.A. Effects of Soluble Lignocellulose Substances of Wood Particles on the Mechanical Properties of Lightweight Concrete. *Int. J. Eng. Technol.* **2018**, *7*, 377. [CrossRef]
41. Camargo, M.; Taye, E.A.; Roether, J.; Redda, D.T.; Boccaccini, A. A Review on Natural Fiber-Reinforced Geopolymer and Cement-Based Composites. *Materials* **2020**, *13*, 4603. [CrossRef]
42. Rihia, C.; Hebhoub, H.; Kherraf, L.; Djebien, R.; Abdelouahed, A. Valorization of Waste in Sand Concrete Based on Plant Fibres. *Civ. Environ. Eng. Rep.* **2019**, *29*, 41–61. [CrossRef]
43. Rao, J.; Zhou, Y.; Fan, M. Revealing the Interface Structure and Bonding Mechanism of Coupling Agent Treated WPC. *Polymers* **2018**, *10*, 266. [CrossRef]
44. Ballesteros, J.E.M.; Santos, S.F.; Mármol, G.; Savastano, H.; Fiorelli, J. Evaluation of Cellulosic Pulps Treated by Hornification as Reinforcement of Cementitious Composites. *Constr. Build. Mater.* **2015**, *100*, 83–90. [CrossRef]
45. Ferreira, S.R.; de Andrade Silva, F.; Lima, P.R.L.; Filho, R.D.T. Effect of Hornification on the Structure, Tensile Behavior and Fiber Matrix Bond of Sisal, Jute and Curauá Fiber Cement Based Composite Systems. *Constr. Build. Mater.* **2017**, *139*, 551–561. [CrossRef]
46. Senthamaraikannan, P.; Kathiresan, M. Characterization of Raw and Alkali Treated New Natural Cellulosic Fiber from Coccinia Grandis.L. *Carbohydr. Polym.* **2018**, *186*, 332–343. [CrossRef] [PubMed]
47. George, M.; Mussone, P.G.; Alemaskin, K.; Chae, M.; Wolodko, J.; Bressler, D.C. Enzymatically Treated Natural Fibres as Reinforcing Agents for Biocomposite Material: Mechanical, Thermal, and Moisture Absorption Characterization. *J. Mater. Sci.* **2016**, *51*, 2677–2686. [CrossRef]
48. Kalia, S.; Thakur, K.; Celli, A.; Kiechel, M.A.; Schauer, C.L. Surface Modification of Plant Fibers Using Environment Friendly Methods for Their Application in Polymer Composites, Textile Industry and Antimicrobial Activities: A Review. *J. Environ. Chem. Eng.* **2013**, *1*, 97–112. [CrossRef]
49. Khelifi, W.; Belouettar, R.; Zeghina, S.I.; Chenia, M.; Daouadji, A.; Azari, Z.; Belouettar, S. Physico-Mechanical Study of an Ordinary Concrete Based On Wood Chips. *J. Mater. Environ. Sci.* **2016**, *7*, 4489–4501.
50. SCHS. Available online: http://www.schs.dz/ (accessed on 4 May 2022).
51. Bogue Calculation. Available online: https://www.understanding-cement.com/bogue.html (accessed on 21 April 2022).
52. Crumbie, A.; Walenta, G.; Füllmann, T. Where Is the Iron? Clinker Microanalysis with XRD Rietveld, Optical Microscopy/Point Counting, Bogue and SEM-EDS Techniques. *Cem. Concr. Res.* **2006**, *36*, 1542–1547. [CrossRef]
53. Labidi, I.; Boughanmi, S.; Tiss, H.; Megriche, A. Critical Research Study of Quantification Methods of Mineralogical Phases in Cementitious Materials. *J. Aust. Ceram. Soc.* **2019**, *55*, 1127–1137. [CrossRef]
54. Shim, S.-H.; Lee, T.-H.; Yang, S.-J.; Noor, N.B.M.; Kim, J.-H.-J. Calculation of Cement Composition Using a New Model Compared to the Bogue Model. *Materials* **2021**, *14*, 4663. [CrossRef]
55. Coussy, S.; Benzaazoua, M.; Blanc, D.; Moszkowicz, P.; Bussière, B. Arsenic Stability in Arsenopyrite-Rich Cemented Paste Backfills: A Leaching Test-Based Assessment. *J. Hazard. Mater.* **2011**, *185*, 1467–1476. [CrossRef]
56. Deschamps, T.; Benzaazoua, M.; Bussière, B.; Aubertin, M.; Belem, T. Microstructural and Geochemical Evolution of Paste Tailings in Surface Disposal Conditions. *Miner. Eng.* **2008**, *21*, 341–353. [CrossRef]

57. Pehanich, J.L.; Blankenhorn, P.R.; Silsbee, M.R. Wood Fiber Surface Treatment Level Effects on Selected Mechanical Properties of Wood Fiber–Cement Composites. *Cem. Concr. Res.* **2004**, *34*, 59–65. [CrossRef]
58. Bédérina, M.; Khenfer, M.M.; Dheilly, R.M.; Quéneudec, M. Reuse of Local Sand: Effect of Limestone Filler Proportion on the Rheological and Mechanical Properties of Different Sand Concretes. *Cem. Concr. Res.* **2005**, *35*, 1172–1179. [CrossRef]
59. Aouissi, H.A.; Ababsa, M.; Gaagai, A.; Bouslama, Z.; Farhi, Y.; Chenchouni, H. Does melanin-based plumage coloration reflect health status of free-living birds in urban environments? *Avian Res.* **2021**, *12*, 45. [CrossRef]
60. Gotteicha, M. Caractérisation Des Bétons de Sable à Base de Copeaux de Bois Traités. Doctoral Dissertation, Centre Universitaire Amar Telidji. Faculté des Sciences et de L'ingenieurie, Laghouat, Algeria, 2005.
61. Lisboa, F.J.N.; Scatolino, M.V.; de Paula Protásio, T.; Júnior, J.B.G.; Marconcini, J.M.; Mendes, L.M. Lignocellulosic Materials for Production of Cement Composites: Valorization of the Alkali Treated Soybean Pod and Eucalyptus Wood Particles to Obtain Higher Value-Added Products. *Waste Biomass Valorization* **2020**, *11*, 2235–2245. [CrossRef]
62. Schaefer, V.R.; Abramson, L.W.; Drumheller, J.C.; Sharp, K.D. *Ground Improvement, Ground Reinforcement and Ground Treatment: Developments 1987–1997*; ASCE: Reston, VA, USA, 1997.
63. Chen, Q.Y.; Tyrer, M.; Hills, C.D.; Yang, X.M.; Carey, P. Immobilisation of Heavy Metal in Cement-Based Solidification/Stabilisation: A Review. *Waste Manag.* **2009**, *29*, 390–403. [CrossRef]
64. You, X.; Hu, X.; He, P.; Liu, J.; Shi, C. A Review on the Modelling of Carbonation of Hardened and Fresh Cement-Based Materials. *Cem. Concr. Compos.* **2022**, *125*, 104315. [CrossRef]
65. Mahmood, W.; Khan, A.-R.; Ayub, T. Carbonation Resistance in Ordinary Portland Cement Concrete with and without Recycled Coarse Aggregate in Natural and Simulated Environment. *Sustainability* **2022**, *14*, 437. [CrossRef]
66. Peter, M.A.; Muntean, A.; Meier, S.A.; Böhm, M. Competition of Several Carbonation Reactions in Concrete: A Parametric Study. *Cem. Concr. Res.* **2008**, *38*, 1385–1393. [CrossRef]
67. Elsalamawy, M.; Mohamed, A.R.; Kamal, E.M. The Role of Relative Humidity and Cement Type on Carbonation Resistance of Concrete. *Alex. Eng. J.* **2019**, *58*, 1257–1264. [CrossRef]
68. Metalssi, O.O.; Aït-Mokhtar, A.; Turcry, P. A Proposed Modelling of Coupling Carbonation-Porosity-Moisture Transfer in Concrete Based on Mass Balance Equilibrium. *Constr. Build. Mater.* **2020**, *230*, 116997. [CrossRef]
69. Chen, X.; Sun, Z.; Pang, J. Effects of Various Corrosive Ions on Metakaolin Concrete. *Crystals* **2021**, *11*, 1108. [CrossRef]
70. Hime, W.G.; Martinek, R.A.; Backus, L.A.; Marusin, S.L. Salt Hydration Distress. *Concr. Int.* **2001**, *23*, 43–50.
71. Feng, P.; Miao, C.; Bullard, J.W. A Model of Phase Stability, Microstructure and Properties during Leaching of Portland Cement Binders. *Cem. Concr. Compos.* **2014**, *49*, 9–19. [CrossRef]
72. Ouyang, W.; Chen, J.; Jiang, M. Evolution of Surface Hardness of Concrete under Sulfate Attack. *Constr. Build. Mater.* **2014**, *53*, 419–424. [CrossRef]
73. Rahman, M.M.; Bassuoni, M.T. Thaumasite Sulfate Attack on Concrete: Mechanisms, Influential Factors and Mitigation. *Constr. Build. Mater.* **2014**, *73*, 652–662. [CrossRef]
74. Tang, S.W.; Yao, Y.; Andrade, C.; Li, Z.J. Recent Durability Studies on Concrete Structure. *Cem. Concr. Res.* **2015**, *78*, 143–154. [CrossRef]
75. Lee, S.T.; Moon, H.Y.; Hooton, R.D.; Kim, J.P. Effect of Solution Concentrations and Replacement Levels of Metakaolin on the Resistance of Mortars Exposed to Magnesium Sulfate Solutions. *Cem. Concr. Res.* **2005**, *35*, 1314–1323. [CrossRef]
76. De Weerdt, K.; Justnes, H. The Effect of Sea Water on the Phase Assemblage of Hydrated Cement Paste. *Cem. Concr. Compos.* **2015**, *55*, 215–222. [CrossRef]
77. Dehwah, H.A.F. Effect of Sulfate Concentration and Associated Cation Type on Concrete Deterioration and Morphological Changes in Cement Hydrates. *Constr. Build. Mater.* **2007**, *21*, 29–39. [CrossRef]
78. Shen, J.; Xu, Q. Effect of Elevated Temperatures on Compressive Strength of Concrete. *Constr. Build. Mater.* **2019**, *229*, 116846. [CrossRef]
79. Araldi, P.; Balestra, C.; Savaris, G. Influence of Multiple Methods and Curing Temperatures on the Concrete Compressive Strength. *J. Eng. Proj. Prod. Manag.* **2019**, *9*, 66. [CrossRef]
80. Ortiz, J.; Aguado, A.; Agulló, L.; García, T. Influence of Environmental Temperatures on the Concrete Compressive Strength: Simulation of Hot and Cold Weather Conditions. *Cem. Concr. Res.* **2005**, *35*, 1970–1979. [CrossRef]
81. El-Zohairy, A.; Hammontree, H.; Oh, E.; Moler, P. Temperature Effect on the Compressive Behavior and Constitutive Model of Plain Hardened Concrete. *Materials* **2020**, *13*, 2801. [CrossRef]
82. Kottititum, B.; Phung, Q.T.; Maes, N.; Prakaypan, W.; Srinophakun, T. Early Age Carbonation of Fiber-Cement Composites under Real Processing Conditions: A Parametric Investigation. *Appl. Sci.* **2018**, *8*, 190. [CrossRef]
83. Ban, Y.; Zhi, W.; Fei, M.; Liu, W.; Yu, D.; Fu, T.; Qiu, R. Preparation and Performance of Cement Mortar Reinforced by Modified Bamboo Fibers. *Polymers* **2020**, *12*, 2650. [CrossRef] [PubMed]
84. AL-Zubaidi, A.B. Effect of Natural Fibers on Mechanical Properties of Green Cement Mortar. *AIP Conf. Proc.* **2018**, *1968*, 020003. [CrossRef]
85. Futami, E.; Shafigh, P.; Katman, H.Y.B.; Ibrahim, Z. Recent Progress in the Application of Coconut and Palm Oil Fibres in Cement-Based Materials. *Sustainability* **2021**, *13*, 12865. [CrossRef]
86. Cho, J.; Waetzig, G.R.; Udayakantha, M.; Hong, C.Y.; Banerjee, S. Incorporation of Hydroxyethylcellulose-Functionalized Halloysite as a Means of Decreasing the Thermal Conductivity of Oilwell Cement. *Sci. Rep.* **2018**, *8*, 16149. [CrossRef]

87. Tonoli, G.H.D.; Filho, U.P.R.; Savastano, H.; Bras, J.; Belgacem, M.N.; Lahr, F.A.R. Cellulose Modified Fibres in Cement Based Composites. *Compos. Part Appl. Sci. Manuf.* **2009**, *40*, 2046–2053. [CrossRef]
88. Malenab, R.; Ngo, J.; Promentilla, M. Chemical Treatment of Waste Abaca for Natural Fiber-Reinforced Geopolymer Composite. *Materials* **2017**, *10*, 579. [CrossRef]
89. Mohr, B.J.; Nanko, H.; Kurtis, K.E. Durability of Kraft Pulp Fiber–Cement Composites to Wet/Dry Cycling. *Cem. Concr. Compos.* **2005**, *27*, 435–448. [CrossRef]
90. Yang, T.; Ma, E.; Cao, J. Effects of Lignin in Wood on Moisture Sorption and Hygroexpansion Tested under Dynamic Conditions. *Holzforschung* **2018**, *72*, 943–950. [CrossRef]
91. Szewczyk, P.K.; Stachewicz, U. The Impact of Relative Humidity on Electrospun Polymer Fibers: From Structural Changes to Fiber Morphology. *Adv. Colloid Interface Sci.* **2020**, *286*, 102315. [CrossRef]
92. De Abreu Neto, R.; Lima, J.T.; Takarada, L.M.; Trugilho, P.F. Effect of Thermal Treatment on Fiber Morphology in Wood Pyrolysis. *Wood Sci. Technol.* **2021**, *55*, 95–108. [CrossRef]
93. Nayeri, M.D. Effects of Temperature and Time on the Morphology, PH, and Buffering Capacity of Bast and Core Kenaf Fibres. *BioResources* **2013**, *8*, 1801–1812. [CrossRef]
94. Mukhopadhyay, S.; Khatana, S. A Review on the Use of Fibers in Reinforced Cementitious Concrete. *J. Ind. Text.* **2015**, *45*, 239–264. [CrossRef]
95. Jiang, S.; Huang, L.; Nguyen, T.A.H.; Ok, Y.S.; Rudolph, V.; Yang, H.; Zhang, D. Copper and Zinc Adsorption by Softwood and Hardwood Biochars under Elevated Sulphate-Induced Salinity and Acidic PH Conditions. *Chemosphere* **2016**, *142*, 64–71. [CrossRef] [PubMed]
96. Bencedira, S.; Bechiri, O. Degradation of Fuchsine Acid Using the HP2W15Mo3Co2.5O62, 20H2O/H2O2 System: Effect of Organic and Inorganic Additives. *Euro-Mediterr. J. Environ. Integr.* **2021**, *6*, 60. [CrossRef]
97. Mold, P.; Godbey, R. Limewash: Compatible coverings for masonry and stucco. In Proceedings of the International Building Lime Symposium, Orlando, FL, USA, 9–11 March 2005.
98. Li, S.; Takasu, C.; Lau, H.; Robles, L.; Vo, K.; Farzaneh, T.; Vaziri, N.D.; Stamos, M.J.; Ichii, H. Dimethyl Fumarate Alleviates Dextran Sulfate Sodium-Induced Colitis, through the Activation of Nrf2-Mediated Antioxidant and Anti-Inflammatory Pathways. *Antioxidants* **2020**, *9*, 354. [CrossRef]
99. Phadagi, R.; Singh, S.; Hashemi, H.; Kaya, S.; Venkatesu, P.; Ramjugernath, D.; Ebenso, E.E.; Bahadur, I. Understanding the Role of Dimethylformamide as Co-Solvents in the Dissolution of Cellulose in Ionic Liquids: Experimental and Theoretical Approach. *J. Mol. Liq.* **2021**, *328*, 115392. [CrossRef]
100. Bao, W.; Jia, Z.; Cai, L.; Liang, D.; Li, J. Fabrication of a Superamphiphobic Surface on the Bamboo Substrate. *Eur. J. Wood Wood Prod.* **2018**, *76*, 1595–1603. [CrossRef]
101. Guerzou, M.; Aouissi, H.A.; Guerzou, A.; Burlakovs, J.; Doumandji, S.; Krauklis, A.E. From the Beehives: Identification and Comparison of Physicochemical Properties of Algerian Honey. *Resources* **2021**, *10*, 94. [CrossRef]
102. Okeyinka, O.M.; Oladejo, O. The Influence of Calcium Carbonate as an Admixture on the Properties of Wood Ash Cement Concrete. *Int. J. Emerg. Technol. Adv. Eng.* **2014**, *4*, 432–437.
103. Merk, V.; Chanana, M.; Gaan, S.; Burgert, I. Mineralization of Wood by Calcium Carbonate Insertion for Improved Flame Retardancy. *Holzforschung* **2016**, *70*, 867–876. [CrossRef]
104. Mejri, W.; Korchef, A.; Tlili, M.; Ben Amor, M. Effects of Temperature on Precipitation Kinetics and Microstructure of Calcium Carbonate in the Presence of Magnesium and Sulphate Ions. *Desalination Water Treat.* **2014**, *52*, 4863–4870. [CrossRef]
105. Bencedira, S.; Bechiri, O.; Djenouhat, M.; Boulkra, M. Cobalt-Substituted Heteropolyanion: Synthesis, Characterization, and Application to Oxidation of an Organic Dye in an Aqueous Medium. *Arab. J. Sci. Eng.* **2020**, *45*, 4669–4681. [CrossRef]
106. Pondelak, A.; Rosi, F.; Maurich, C.; Miliani, C.; Škapin, S.D.; Sever Škapin, A. The Role of Relative Humidity on Crystallization of Calcium Carbonate from Calcium Acetoacetate Precursor. *Appl. Surf. Sci.* **2020**, *506*, 144768. [CrossRef]
107. Graine, R.; Bedoud, K.; Sehab, N.; Zelmati, D. Influence of the substrate temperature on tio2 thin layers deposited by the direct current magnetron sputtering technology. *Surf. Rev. Lett. SRL* **2021**, *28*, 2050054. [CrossRef]
108. Zhang, S.Y.; Ren, H.; Jiang, Z. Wood Density and Wood Shrinkage in Relation to Initial Spacing and Tree Growth in Black Spruce (Picea Mariana). *J. Wood Sci.* **2021**, *67*, 30. [CrossRef]